Characterization of ground and excited electronic state deprotonation energies of systems containing double bonds using natural bond orbital analysis

Jay K. Badenhoop and Steve Scheiner
Department of Chemistry, Southern Illinois University, Carbondale, Illinois 62901

Natural bond orbital analysis is applied to the ground and excited states of a set of neutral, cationic, and anionic doubly bonded species $H_nC{=}XH_n$ (X=C, N, O) isoelectronic with ethylene. The character of the excitation is correlated with calculated charge shifts and geometry changes upon relaxation. For these planar molecules, depopulation of the π bond or population of the π^* antibond causes an out-of-plane twist or pyramidalization upon relaxation correlated to the amount of charge shift. These nonplanar distortions generally lower the energy more than changes in bond lengths and angles. Population of a σ^*_{XH} antibond by more than ${\sim}0.4\ e$ often leads to dissociation of that proton. The character and symmetry of the transition are used to match excited states in the protonated and deprotonated species so as to extract an excited state deprotonation energy. The vertical deprotonation energy of the $\pi{\to}\pi^*$ state tends to be higher than that of the ground state due to greater electronic destabilization of the deprotonated species, while Rydberg excited states take less energy to deprotonate. Adiabatic deprotonation energies can be greater or less than that of the ground state depending on whether the protonated or deprotonated species is more stabilized by geometry relaxation. © *1996 American Institute of Physics.* [S0021-9606(96)01835-1]

I. INTRODUCTION

The topic of proton transfer has received much attention because of its importance in many chemical and biological processes, including solvation,[1] enzyme catalysis,[2] and ion transport.[3] The phenomenon of photoinduced proton transfer has been studied experimentally[4] and, with the development of *ab initio* methods for the calculation of excited state wave functions[5,6] and including correlation,[7] a variety of intermolecular and intramolecular proton transfer reactions have been studied theoretically.[8] Electronic excitation alters the properties of the system so as to enable rapid transfer.

Probably the most dominant of these properties is the gas-phase proton affinity or deprotonation energy of the proton donor and acceptor groups, which reflects their intrinsic basicity in the absence of any solvent effects. A systematic, detailed study of the effect of excited state electronic and geometric rearrangement on the proton affinities of simple groups might be expected to shed light on the factors that control excited state proton transfer. One such set of molecules are those that contain doubly bonded C, N, and O atoms in a planar unsaturated group, many of which are known chromophores.[9]

Several detailed calculations of accurate vertical and adiabatic transition energies for both valence and Rydberg excited states of ethylene[5,10,11,15] and formaldehyde[5,12–16] have been recently performed. Early experimental work, reviewed by Merer and Mulliken,[17] identified five important states in ethylene: $^1A_1$ (ground state), $^3B_{1u}$ (triplet $\pi{\to}\pi^*$ state), $^3B_{3u}$ (triplet $\pi{\to}3s$ Rydberg state), $^1B_{3u}$ (singlet $\pi{\to}3s$), and $^1B_{1u}$ (singlet $\pi{\to}\pi^*$), or *N* (normal), *T* (lowest triplet), T_R (triplet Rydberg), *R* (singlet Rydberg), and *V* (lowest singlet), respectively, in Mulliken's notation. CIS

calculations by Foresman *et al.*[5] showed the two $\pi{\to}\pi^*$ states are both stabilized by torsional "twisting" from the planar D_{2h} structure to a D_{2d} structure with the two CH_2 planes oriented 90° with respect to each other, along with a lengthening of the CC bond.

Formaldehyde, the simplest in the class of carbonyl compounds, shows both $\pi{\to}\pi^*$ and $n{\to}\pi^*$ transitions, important for photochemical reactions, due to the presence of both the π system and two oxygen lone pairs. Hadad *et al.*[14] calculated the vertical transition energies for the first 20 singlet states and 10 triplet states. The adiabatic $\pi{\to}\pi^*$ singlet state is planar, but with a longer CO bond length, and the triplet $\pi{\to}\pi^*$ and $n_y{\to}\pi^*$ states distort to a nonplanar geometry. While the second highest occupied molecular orbital (labeled π) is essentially a localized π bond, the HOMO (labeled n_y) was found to be not simply a nonbonding oxygen lone pair as stated previously,[18] but actually delocalized over the entire molecule. However, charge density difference plots showed several pairs of excitations with the same symmetry to be mixtures of $\pi{\to}\pi^*$ and $n{\to}3p$ character, requiring some states to have more than one label. The molecular orbitals of acetaldehyde, with just an additional methyl group, were found to have an even greater amount of mixing, such that labels "π" and "n" no longer fully describe the character of the state (but were used for consistency with earlier work).

In addition to the comprehensive body of work on $H_2C{=}CH_2$ and $H_2C{=}O$, the energetics of other selected doubly bonded species isoelectronic with ethylene have been studied. Ground state proton affinities have been calculated for the ethylene anion, $H_2C{=}CH^-$,[19–21] formaldehyde,[20–28] and $H_2C{=}NH$[20,23,29] semiempirically,[22,25,29] at various levels
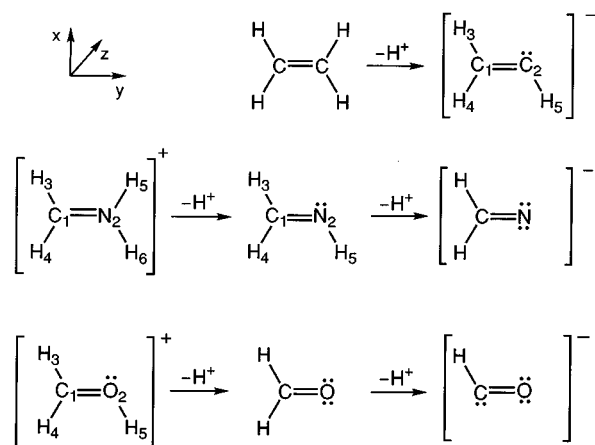
FIG. 1. Deprotonation reactions of doubly bonded species considered in this study.

of *ab initio* theory,[19,23,24,26–28] and using several density functional methods.[27]

Calculations by Marudarajan and Scheiner on the ground and excited states of HC≡CH[30] and HC≡N[31] and their deprotonated anions at the unrestricted Hartree–Fock (UHF) and unrestricted Møller–Plesset (UMP2) level showed that these species undergo a radical change in geometry upon excitation to low-lying excited states, from linear to bent. The lower energy of the acetylene $\pi \rightarrow \pi^*$ bent conformation was explained using the molecular orbital (MO) atomic orbital coefficients; the π^* MO, whose greatest contribution is from the hydrogens, is stabilized by moving these atoms to either the *trans* or *cis* position. The excited states of HC≡N require several kcal/mol more energy to deprotonate than the ground state, consistent with a shift in electron density toward the carbon center. However, despite a strong shift in density from C to H, the deprotonation energies of the first singlet and first two triplet states of acetylene are nearly the same as for the ground state. For both molecules, the difference in the deprotonation energies is less than 5% of the ground state value. It is not clear from these two examples whether this is a general phenomenon, or peculiar to simple triply bonded molecules.

The current paper reports the study, at a satisfactory *ab initio* level of theory, of the ground and low-lying excited states of a subset of neutral doubly bonded species $H_2C=XH_n$ (X=C, N, O; n=2,1,0) isoelectronic with ethylene, and the cations and anions that result from protonation and deprotonation, respectively. The relevant deprotonation reactions are shown in Fig. 1. We wish to determine the generality of the isolated results of previous studies of these species, as well as to determine trends in proton affinities based on the character of the state as the electronegativity of the X atom increases and XH bonds are replaced with lone pairs. This set of molecules was chosen because the ground state is well described by one localized set of Lewis-type bonding orbitals, and the ground state planar geometry allows clear separation between the σ and π systems to be retained in the vertically excited states.

In both HC≡CH and HC≡N, the low-lying valence excited states could be easily correlated between the protonated and deprotonated species because the states were spread fairly far apart and had unique symmetry. This may not usually be the case, and a more systematic method of correlating excited states of similar character is needed. Natural orbital analysis (NBO)[32,33] is used here to assign the character of each excited state by describing the density in terms of a set of easily recognizable Lewis-type bonding orbitals. This process allows corresponding excited state energies in the protonated and deprotonated species to be ''matched'' to yield deprotonation energies even in species with a high density of electronic states. We investigate the generality of the geometry changes observed for the adiabatic excited states of ethylene and formaldehyde in states of similar character over the $H_2C=XH_n$ isoelectronic series, and suggest the origin of these changes based on the excited state character and the orbitals affected by the excitation.

II. METHOD

For consistency, the coordinates for all molecules in this study were transformed as indicated in Fig. 1. The z axis is perpendicular to the plane of the molecule, x is in-plane perpendicular to the C–X bond, and the y axis is parallel to the C–X bond. All calculations were performed using the GAUSSIAN 92[34] electronic structure package. The 6-31 +G(d,p) basis set[35] was chosen as the smallest basis set that includes both polarization functions on all atoms ($3d$ orbitals on C, N, O; $2p$ on H) and diffuse sp functions on heavy atoms,[23,36] needed to properly describe anions,[23,36] certain Rydberg excited states,[5,14] and proton affinities of neutral species with nonbonding electron pairs.[37] This basis has also been shown to have a particularly low basis set superposition error (BSSE) among available standard basis sets.[38,39] McMurchie and Davidson,[40] who used a similar basis for calculations on ethylene, commented that the use of an even more complete basis would clutter the π^* subspace, as well as obscure identifiable contributions from σ^* valence orbitals. Indeed, despite yielding more accurate vertical transition energies, many excited states could not be optimized at the 6-311(2+)G** level because of multiple curve crossings by the larger manifold of Rydberg states during the relaxation process. The 6-31+G(d,p) basis was the largest one which allowed clear optimization of the valence states.

The ground state geometries were optimized at the restricted Hartree–Fock (RHF) level of theory. Energies of the first 10 singlet and triplet vertical transitions for cations and neutral species (which includes the most important valence and Rydberg states) and the first 15 transitions for anions (or those with transition energies up to ~200 kcal/mol) were then computed by the CIS (configuration interaction among all single excitations) method.[5,15,41] The excited states were next allowed to relax to their optimized geometry at the CIS level, yielding an adiabatic excitation energy.

The CIS method has been successfully applied to the excited states of a variety of molecules[42] including the ethylene and formaldehyde studies mentioned above.[5,10,14] Even with a basis containing diffuse functions, the excited state transition energies tend to be consistently too high by a few kcal/mol for valence states, and by as much as 23 kcal/mol for Rydberg states. Applying Møller–Plesset second-order perturbations (MP2) to the CIS wave function brought the excited state energies of formaldehyde more in line with experiment.

Our analysis of excited state densities showed that while atomic orbitals based on the CIS generalized density have reasonable occupancies and overlap matrix elements, densities from both the CIS-MP2 and spin unrestricted form of the CIS wave function (UCIS) yield unreliable populations. The occupancies of several of the atomic orbitals (AOs) formed from these densities are negative, and overlaps of the resulting LCAO bond orbitals with one another are several times larger than for ground state densities. The occupancy-weighted symmetric orthogonalization of these AOs to form natural bond orbitals[32] yields populations significantly outside the expected range of 0–2 electrons,[43,44] making the assignment of excited state character based on such natural bond orbitals (NBOs) unreliable for the purpose of correlating states between protonated and deprotonated species. To avoid this problem we have consistently retained the CIS level to ascertain qualitative and quantitative trends.

Natural bond orbital (NBO) analysis of the ground state and excited state densities was performed separately in order to show the shift in electron density upon excitation, independent of the choice of ground state orbitals. NBOs are the localized set of easily recognizable Lewis-like (σ and π bond, lone pair, and core) and non-Lewis (σ^* and π^* antibond and Rydberg) orbitals which are optimal in the sense of orthonormality and maximum occupancy of the Lewis set. The total non-Lewis density (ρ^*), or sum of occupancies of the non-Lewis orbitals, is a measure of the degree of delocalization. There is also a clear distinction between valence and Rydberg orbitals, so that the character can be easily seen in the orbital labels and occupancies, and from the total Rydberg occupancy. If both the occupied and unoccupied MOs involved in the excitation are localized on one or two centers, e.g. for $\pi \rightarrow \pi^*$ excitation, then the NBOs not involved in the excitation can be expected to be nearly identical in shape and occupancy to the corresponding ground state orbitals, and only the two corresponding NBOs should be of different form and with depleted bond occupancy and increased antibond occupancy. If the excitation involves MOs with density on several centers, then the optimal set of occupied (Lewis) NBOs will be somewhat different in shape and of lower occupancy to reflect the depletion of density in the bonding regions, while several non-Lewis orbitals will have higher occupancy. Therefore analysis of the differences between the two sets of NBOs shows directly the extent to which the excitation is delocalized.

III. EXCITED STATE DENSITIES AND DEPROTONATION ENERGIES

A. Ethylene

Table I lists the most important singlet and triplet valence and Rydberg excited states of ethylene along with the corresponding transition energies. We consider first the vertical transitions. Each state is characterized by both the symmetry of the transition and the corresponding molecular orbitals as characterized by changes in NBO populations. (Mulliken's labels for the T, V, T_R, and R states are also indicated.) Included in the label are all NBOs which are populated or depopulated by at least 0.1 e compared with the ground state NBOs, in decreasing order of the magnitude of the change in occupancy. Most of the ethylene excitations are fairly localized, involving significant changes to only 2–4 NBOs.[45] For ethylene, the HOMO is essentially the π_{CC} bond; hence most of the low-lying singlet and triplet states depopulate the π_{CC} NBO. The second highest occupied MO consists of a linear combination of the σ_{CC} and σ_{CH} bonds; states which excite from this MO have weaker σ_{CH} NBOs with an occupancy of only 1.74–1.84 e compared to 1.987 for the ground state. For the ninth singlet and triplet states, a σ_{CC} orbital with 1.56–1.60 e, depleted from 1.997, is also involved.

CIS calculations using a basis set with two sets of diffuse functions [6-311(2+)G*] were performed on ethylene by Wiberg et al.[10] In contrast to our NBO analysis, charge density difference plots were used to assign the character of the first 20 singlet and 10 triplet states of ethylene. Accounting for the axis rotation from C_{2v} to C_s symmetry ($x \rightarrow z, y \rightarrow x, z \rightarrow y$), our ordering and assignments of the valence and $\pi \rightarrow r_{3s}$ and $\pi \rightarrow r_{3p}$ Rydberg states are fairly close to theirs (though slightly higher in energy), listed in the fifth column of Table I. However, they assigned the $2\,^1B_{1g}$ and $2\,^3B_{1g}$ states as $\pi'_{CH_2} \rightarrow \pi^*$, whereas we find that these states clearly depopulate the σ_{CH} and σ_{CC} orbitals, and the MO has no π character. The only exception in ordering is the energy reversal of the $1\,^1B_{1u}$ and $1\,^1B_{1g}$ states, although their two states lie within 1 kcal/mol of one another. The singlet states were found by Wiberg et al. to be more diffuse and higher in energy than the triplet states of the same character, which also agrees with our results. They also found a significant decrease in CC bond order for the $\pi \rightarrow \pi^*$ and Rydberg states, consistent with weakening of the π bond.

Listed in the sixth column of Table I are the changes in the natural atomic charges[32(c)] of the carbon atoms upon excitation. The sixth and ninth singlet and triplet states manifest a noticeable charge shift away from H and toward C, consistent with depopulation of the CH bonds. This finding is understandable in light of the shift out of the σ_{CH} NBOs and into π^*_{CC} or a C Rydberg orbital. The NBO analysis of both the $1\,^1B_{1u}(V)$ and $2\,^1A_g$ singlet states confirms significant mixing of π^* and Rydberg character, previously found by Buenker and Peyerimhoff,[46] Robin,[47] and Mulliken.[48]

The excited states of ethylene can be compared with those of its deprotonated form, CH_2CH^-, reported in Table II. One CH bond of ethylene has been replaced with a more

TABLE I. Vertical excitation energies (VEE in kcal/mol), natural charge shifts, adiabatic excitation energies (AEE), and optimized geometries[a] for ethylene.

State	Symmetry[b]	Transition[c]	VEE[d]	Wiberg[e]	Δq_c[f]	AEE	r_{CC}	r_{CH}	θ_{CCH}
Ground state									
0	$1\,^1A_g(N)$						1.3206	1.0764	121.66
Singlet states									
1	$1\,^1B_{3u}(R)$	$\pi_{CC} \rightarrow r_{C(3s)}(2)$	179.7	164.4	+0.037	174.0	1.4121	1.0714	120.31
2[g]	$1\,^1B_{1u}(V)$	$\pi_{CC} \rightarrow \pi^*_{CC}/r_{C(3p_z)}(2)$	182.4	178.5	−0.024	130.4	1.3747	1.0897	123.64
3	$1\,^1B_{1g}$	$\pi_{CC} \rightarrow r_{C(3p_x)}(2)$	189.9	177.8	+0.068	185.6	1.3983	1.0784	119.36
4	$1\,^1B_{2g}$	$\pi_{CC} \rightarrow r_{C(3p_y)}(2)$	192.7	181.3	−0.014	185.3	1.4297	1.0742	121.46
5[h]	$2\,^1A_g$	$\pi_{CC} \rightarrow r_{C(3p_z)}(2)/\pi^*_{CC}$	209.2	186.6	−0.057	203.3	1.3753	1.0779	120.60
6	$2\,^1B_{1g}$	$\sigma_{CH}(4) \rightarrow \pi^*_{CC}$	216.9	214.0	−0.301	unresolvable curve crossing			
9	$2\,^1B_{2g}$	$\sigma_{CC}/\sigma_{CH}(4) \rightarrow \pi^*_{CC}$	242.1	236.6	−0.140	195.7	1.6330	1.0676	108.30
Triplet states									
1[i]	$1\,^3B_{1u}(T)$	$\pi_{CC} \rightarrow \pi^*_{CC}$	85.8	82.3	+0.070	49.6	1.4605	1.0762	121.26
2	$1\,^3B_{3u}(T_R)$	$\pi_{CC} \rightarrow r_{C(3s)}(2)$	170.5	159.3	+0.021	163.9	1.4182	1.0699	120.06
3	$1\,^3B_{1g}$	$\pi_{CC} \rightarrow r_{C(3p_x)}(2)$	186.6	175.9	+0.085	182.6	1.3941	1.0817	119.54
4	$1\,^3B_{2g}$	$\pi_{CC} \rightarrow r_{C(3p_y)}(2)$	188.6	178.7	+0.008	179.8	1.4498	1.0806	121.71
5	$1\,^3A_g$	$\pi_{CC} \rightarrow r_{C(3p_z)}(2)$	191.4	179.2	−0.078	186.8	1.4007	1.0706	120.38
6	$2\,^3B_{1g}$	$\sigma_{CC}/\sigma_{CH}(4) \rightarrow \pi^*_{CC}$	201.2	197.4	−0.300	Unresolvable curve crossing			
9[j]	$2\,^3B_{2g}$	$\sigma_{CH}(4)/\sigma_{CC} \rightarrow \pi^*_{CC}$	225.2		−0.151	170.1	1.4638	1.1191	87.29
								1.0753	129.46

[a]Distances are in angstroms, and angles are in degrees.
[b]State symmetry in ground state geometry.
[c]Numbers in parentheses indicate number of such orbitals involved, e.g., orbitals on both C atoms.
[d]This work.
[e]Reference 10, CIS/6-311(2+)G**.
[f]$\Delta q_H = -1/2\Delta q_C$.
[g]$\phi_{H_5CCH_3} = 88.40°$ ("twist" dihedral angle, degrees from planarity).
[h]$\phi_{H_5CCH_3} = 33.32°$.
[i]$\phi_{H_5CCH_3} = 85.70°$.
[j]$\phi_{H_5CCH_3} = 16.75°$, $\phi_{H_4CCH_3} = 54.62°$ ("pyramidal distortion" dihedral angle, degrees from planarity).

flexible (and higher energy) carbon lone pair, which becomes the primary contributor to the HOMO. Lone pair NBOs are labeled italic n, which should not be confused with nonbonding orbitals (n) which refer to MO types. The first excited singlet state shows evidence of valence-Rydberg mixing similar to that in some of the $\pi \rightarrow \pi^*$ excitations in ethylene. The anion's transition energies are lower and closer together than in the neutral.

The nonequivalence of the two C atoms in CH_2CH^- leads to substantial shifts of density from one to the other. The n_{C_2} NBO is of course heavily localized on C_2, the carbon bonded to one hydrogen. Hence those states exciting out of this orbital tend to shift density from C_2 toward C_1. The first triplet, for example, shows charge shifts on C_1 and C_2 in excess of 0.3. (The hydrogens are also affected, but to a lesser extent.) Though the ground state C–C π bond is polarized 64%/36% toward C_1 (and therefore the π^* toward C_2), π excitations sometimes also shift charge in the same direction. C_1 gains half of an electron in the third singlet. States which show a charge buildup on C_2 generally excite into a Rydberg orbital of that atom. Overall, one can conclude that electronic excitation affects charge distribution quite differently in the neutral and anionic forms of ethylene.

Allowing relaxation of the molecular geometries following electronic excitation leads to certain important changes. Table I reports the adiabatic excitation energies (AEE) and optimized geometries for the excited states of ethylene in the last columns. These structures may be compared to the ground state geometry in the first row. Nearly every excitation lengthens the CC bond. This is not surprising since excitation out of the π bond or into the π^* antibond weakens the CC bond and causes it to elongate. The only state in which the CC bond is shorter is the B_{3g} singlet excited state, which depopulates the CH bonds and moves density from the hydrogens to the carbons. The CH bond length is fairly insensitive to excitation except when the CC bond length undergoes a sizable change. The same is true of the CCH angle. A longer r_{CC} tends to shorten r_{CH} and push the CH bonds further apart, i.e., θ_{CCH} decreases.

The largest increase in bond length is seen in the $2\,^1B_{2g}$ singlet state, in which the σ_{CC} bond is depopulated in addition to the π^*_{CC} occupation. $\pi \rightarrow \pi^*$ excitations, as in $^1B_{1u}$ and $^3B_{1u}$, completely sever the π bond and the molecule twists out of a planar structure to a staggered conformation nearly of D_{2d} symmetry (90° twist), shown in Fig. 2(a). Though an electron is excited out of the π bond for both states, the fifth singlet transition populates the π^* orbital to a lesser extent (0.118 e) than the second (0.921 e), and so the torsional twist is less, only 33° from planar [Fig. 2(b)]. The greatest distortion is seen for the ninth triplet state ($\sigma_{CH}/\sigma_{CC} \rightarrow \pi^*$); the optimized geometry is shown in Fig. 2(c). The CH_2 groups are not only twisted relative to each

TABLE II. Vertical excitation energies (kcal/mol), natural charge shifts,[a] adiabatic excitation energies, and optimized geometries for CH_2CH^-.

State	Symmetry	Transition	VEE	Δq_{C_1}	Δq_{C_2}	AEE	r_{CC}	r_{CH_5}
Ground state								
0	$1\,^1A'$						1.3544	1.1062
Singlet states								
1[b]	$1\,^1A''$	$n_{C_2} \to \pi^*_{CC} r_{C_1(3p_z)} / r_{C_2(3p_z)}$	92.7	-0.331	$+0.132$	65.1	1.3975	1.0873
2	$2\,^1A'$	$n_{C_2} \to r_{C_2(3sp_{xy})}$	99.2	-0.044	-0.087	74.6	1.3938	1.0661
3	$3\,^1A'$	$n_{C_2} \to r_{C_1(3sp_y)} / r_{C_2(3sp_y)}$	105.6	-0.502	$+0.233$	87.2	1.2754	1.0681
4	$2\,^1A''$	$\pi_{CC} \to r_{C_1(3sp_y)}$	114.5	-0.260	$+0.006$	109.0	1.4515	1.0955
5	$4\,^1A'$	$n_{C_2} \to r_{C_1(3p_x)} / r_{C_2(3p_x)}$	119.1	-0.389	$+0.201$	Unresolvable curve crossing		
6	$3\,^1A''$	$n_{C_2} \to r_{C_1(3p_z)} / r_{C_2(3p_z)}$	120.6	-0.135	-0.115	103.1	1.2780	1.0684
7	$5\,^1A'$	$\pi_{CC} \to r_{C_1(3p_x)} / r_{C_2(3p_x)}$	131.6	-0.140	$+0.167$	103.9	1.2767	1.0724
8	$6\,^1A'$	$n_{C_2}/\pi_{CC}/\sigma_{CH_5} \to r_{C_2(3p_x)}/r_{C_1(3p_z)}/r_{C_1(3p_x)}$	136.1	-0.228	$+0.082$	131.0	1.3287	1.0786
11	$8\,^1A'$	$\pi_{CC}/n_{C_2} \to r_{C_1(3p_z)}/r_{C_2(3p_z)}/\pi^*_{CC}$	150.0	-0.090	-0.008	147.4	1.4028	1.0897
12	$5\,^1A''$	$\pi_{CC}/n_{C_2} \to \pi^*_{CC}/r_{C_1(3p_z)}/r_{C_2(3p_z)}$	161.2	-0.072	$+0.011$	160.4	1.3800	1.0949
13	$6\,^1A''$	$\pi_{CC} \to r_{C_2(3p_{xy})}/r_{C_1(3sp_{xy})}$	166.3	$+0.067$	-0.123	160.7	1.4543	1.0956
Triplet states								
1[c]	$1\,^3A''$	$n_{C_2} \to \pi^*_{CC}$	65.1	-0.440	$+0.320$	41.1	1.4518	1.0970
2	$1\,^3A'$	$n_{C_2} \to r_{C_2(3s)}$	82.6	$+0.035$	-0.225	66.8	1.2978	1.0596
3[c]	$2\,^3A''$	$\pi_{CC} \to \pi^*_{CC}$	88.6	$+0.376$	-0.309	41.1	1.4518	1.0970
4	$2\,^3A'$	$n_{C_2} \to r_{C_1(3sp_{xy})}/r_{C_2(3sp_{xy})}/\sigma^*_{CH_5}$	101.4	-0.355	$+0.151$	83.3	1.2739	1.0726
5	$3\,^3A'$	$n_{C_2} \to r_{C_2(3p_x)}/r_{C_1(3sp_{xy})}/\sigma^*_{CH_5}$	104.1	-0.106	-0.107	66.8	1.2978	1.0596
6	$4\,^3A'$	$\pi_{CC} \to r_{C_1(3sp_y)}$	108.5	-0.271	$+0.279$	83.3	1.2739	1.0726
7	$3\,^3A''$	$n_{C_2} \to r_{C_1(3p_z)}/r_{C_2(3p_z)}$	115.5	-0.052	-0.183	98.7	1.2806	1.0675
8[d]	$5\,^3A'$	$\pi_{CC} \to r_{C_1(3p_z)}/r_{C_2(3p_z)}/\pi^*_{CC}$	126.9	-0.321	$+0.206$	123.1	1.4297	1.0917
9	$6\,^3A'$	$\pi_{CC} \to r_{C_1(3p_{xy})}/r_{C_2(3sp_x)}$	127.4	-0.132	$+0.139$	98.7	1.2806	1.0675
13	$5\,^3A''$	$\pi_{CC}/n_{C_2} \to r_{C_2(3p_y)}/\pi^*_{CC}/r_{C_1(3p_y)}/r_{C_2(3p_z)}$	159.2	-0.056	-0.074	154.0	1.4562	1.0883

[a] C_1 is bonded to two hydrogens and C_2 to one in CH_2CH^-.
[b] $\phi_{H_5CCH_3} = 74.06°, \phi_{H_4CCH_3} = 31.86°$.
[c] $\phi_{H_5CCH_3} = 55.37°, \phi_{H_4CCH_3} = 48.36°$
[d] $\phi_{H_5CCH_3} = 1.87°, \phi_{H_4CCH_3} = 2.10°$.

other, but also pyramidalized 55° away from planar. Nonplanar distortions generally lower the adiabatic excitation energy more than planar geometry changes, leading to a reordering relative to the vertical excitations. CIS-MP2/6-31+G* optimization[5] of the first singlet $\pi \to 3s$ (R) state relaxed the geometry to a D_2 structure twisted by 24°, compared to 37° for experiment;[49] the CC bond also

CH_2CH_2

a) singlet 2 ($^1B_{1u}$)
   triplet 1 ($^3B_{1u}$)
b) singlet 5 (^1A_g)
c) triplet 9 ($^3B_{2g}$)

CH_2CH^-

d) singlet 1 ($^1A''$)
e) triplet 1 ($^3A''$)

FIG. 2. Nonplanar excited state geometries (CIS 6-31+G*) of CH_2CH_2 and CH_2CH^-.

lengthened to 1.41 Å and the HCH angle increased by 3.0°. The CIS method without correlation finds a planar optimized geometry for the $\pi \to r_{C(3s)}$ states, though the surface is relatively flat relative to out-of-plane twist. More specifically, the CIS energy of the R state at the CIS/MP2 optimized value of $\phi = 23.66°$ lies only 0.66 kcal/mol above that of the planar geometry.

Table II lists the optimized CC and $C-H_5$ bond lengths and HCCH rotation angles for CH_2CH^-. Optimized geometries for some excited states could not be found, particularly in states involving changes in the torsion angle. In these cases the given CIS root shows mixing of several occupied and unoccupied MOs, and the optimization procedure cannot follow the excited state across multiple curve crossings. This occurs more often for cations and anions than for neutral species. One also sees more than one state converge to the same geometry when optimization occurs. An example of this is the pair of $^3A'$ states numbered 2 and 5. As in the case of ethylene, strong excitation into the CH_2CH^- π^* antibond often leads to nonplanar distortion of the molecule, as in the first singlet and triplet states [Figs. 2(d) and 2(e)], or a large increase in CC bond length. However, unlike CH_2CH_2 itself the anionic species can relax to relieve steric strain by increasing the CCH_5 bond angle from the ground state value of 108.57° to the more linear 140°–149° observed in many of the Rydberg excited states.
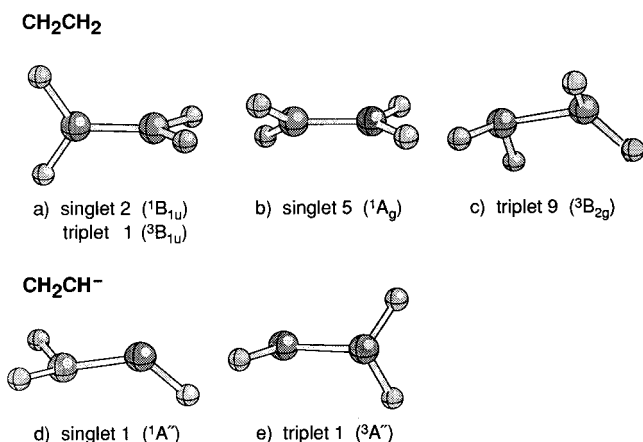
TABLE III. Vertical excitation energies (kcal/mol), adiabatic excitation energies, and optimized geometries for $CH_2NH_2^+$.

State	Symmetry	Transition	VEE	AEE	r_{CN}	r_{CH}[a]	r_{NH}[a]	θ_{NCH}	θ_{HNC}
Ground state									
0	$1\,^1A_1$				1.2633	1.0761	1.0043	119.81	121.70
Singlet states									
1[b]	$1\,^1A_2$	$\pi_{CN}/\sigma_{CH}(2) \to \pi^*_{CN}$	206.2	114.8	1.3165	1.0902	1.0145	121.15	122.90
2[b]	$2\,^1A_1$	$\pi_{CN} \to \pi^*_{CN}$	234.4	114.8	1.3165	1.0902	1.0145	121.15	122.90
3[b]	$1\,^1B_1$	$\sigma_{CN}/\sigma_{CH}(2)/\pi_{CN}/\sigma_{NH}(2) \to \pi^*_{CN}$	271.2	114.8	1.3165	1.0902	1.0145	121.15	122.90
4[b]	$2\,^1B_1$	$\pi_{CN} \to r_{N(3s)}/\sigma^*_{NH}(2)$	278.6	114.8	1.3165	1.0902	1.0145	121.15	122.90
5	$2\,^1A_2$	$\pi_{CN} \to r_{N(3p_x)}/\sigma^*_{NH}(2)$	298.4	280.1	1.3255	1.0975	1.1895	120.08	126.51
6[b]	$1\,^1B_2$	$\sigma_{CH}(2)/\sigma_{NH}(2) \to r_{C(3s)}/r_{N(3s)}/\sigma^*_{NH}(2)/\sigma^*_{CH}$	322.5	114.8	1.3165	1.0902	1.0145	121.15	122.90
7[b]	$3\,^1B_1$	$\pi_{CN} \to r_{C(3sp_y)}/r_{N(3p_y)}/\sigma^*_{CH}(2)$	327.5	114.8	1.3165	1.0902	1.0145	121.15	122.90
8	$3\,^1A_2$	$\pi_{CN}/\sigma_{NH}(2) \to \pi^*_{CN}$	333.4	280.1	1.3255	1.0975	1.1895	120.08	126.51
9[c]	$3\,^1A_1$	$\pi_{CN} \to r_{N(3p_z)}/r_{C(3p_z)}/\pi^*_{CN}$	340.4	318.3	1.3026	1.1225	1.0338	118.72	121.72
10	$2\,^1B_2$	$\sigma_{CH}(2)/\sigma_{NH}(2) \to r_{C(3p_z)}$	350.3	Dissociative—C–H bonds broken					
Triplet states									
1[d]	$1\,^3A_1$	$\pi_{CN} \to \pi^*_{CN}$	124.2	92.2	1.3658	1.0931	1.0159	110.50	124.00
						1.0781	1.0142	115.95	120.42
2[d]	$1\,^3A_2$	$\pi_{CN}/\sigma_{CH}(2) \to \pi^*_{CN}/\sigma^*_{CH}(2)$	183.2	92.2	1.3658	1.0781	1.0142	115.95	120.42
						1.0781	1.0142	115.95	120.42
3[d]	$1\,^3B_1$	$\pi_{CN}/\sigma_{CN}/\sigma_{CH}(2) \to \pi^*_{CN}$	243.6	92.2	1.3658	1.0781	1.0142	115.95	120.42
						1.0781	1.0142	115.95	120.42
4	$2\,^3B_1$	$\pi_{CN} \to \sigma^*_{NH}(2)/r_{N(3s)}$	264.6	Dissociative N–H bond broken					
5	$2\,^3A_2$	$\pi_{CN} \to \sigma^*_{NH}(2)/r_{N(3p_x)}$	291.4	Dissociative—N–H bond broken					
6	$1\,^3B_2$	$\sigma_{CH}(2)/\sigma_{NH}(2) \to \sigma^*_{CH}(2)/r_{C(3sp_y)}$	298.2	Dissociative—C–H bond broken					
7	$2\,^3A_1$	$\sigma_{CH}(2)/\sigma_{NH}(2) \to \sigma^*_{CH}(2)/\sigma^*_{NH}(2)$	309.7	Dissociative—C–H bond broken					
8	$3\,^3A_2$	$\pi_{CN}/\sigma_{NH}(2) \to \pi^*_{CN}/\sigma^*_{NH}(2)$	318.6	Unresolvable curve crossing					
9[d]	$3\,^3B_1$	$\pi_{CN} \to r_{C(3s)}/r_{N(3p_y)}/\sigma^*_{CH}(2)$	318.9	92.2	1.3658	1.0931	1.0159	110.50	124.00
						1.0781	1.0142	115.95	120.42
10	$2\,^3B_2$	$\sigma_{CH}(2)/\sigma_{NH}(2) \to \sigma^*_{NH}(2)/r_{C(3p_y)}$	320.5	Dissociative—N–H bond broken					

[a]Triplet states optimize to C_1 geometry; first row = r_{CH_1}, r_{NH_3}; second row = r_{CH_2}, r_{NH_4}

[b]$\phi_{H_5NCH_4} = 90.00°$.

[c]$\phi_{H_5NCH_4} = 56.24°$.

[d]$\phi_{H_5NCH_4} = 81.05°$, $\phi_{H_4CNH_3} = 48.04°$.

B. CH₂NH

Table III lists the excited states of $CH_2NH_2^+$, which has the same basic geometry as ethylene except that one carbon is replaced by the more electronegative N. Like ethylene, most of the excitations come from the π HOMO. The low-lying excitations in $CH_2NH_2^+$ involve π^*, as compared to the Rydberg transitions of CH_2CH_2. Compared with ethylene, excitations of $CH_2NH_2^+$ are less localized, with more of them involving MOs which include the CH and NH bonds and antibonds in addition to the π_{CN} or π^*_{CN} orbitals. The vertical excitation energies are spread further apart for this cation than for ethylene, with the Rydberg excitations occurring higher in the list relative to the valence excitations.

Table IV shows the excited states of neutral CH_2NH. As in the CH_2CH_2/CH_2CH^- case, removal of a proton from $CH_2NH_2^+$ reduces the spacing of the excited state energy levels. Nearly every excitation shifts electron density from N to C, similar to $C_2 \to C_1$ shifts in CH_2CH^-. The greatest charge shifts from N to C, 0.38–0.53 e, are seen in excitations from the nitrogen lone pair to a carbon Rydberg orbital. Also significant are excitations into the π^* orbital, which is polarized toward carbon.

Removal of a second proton to form CH_2N^- produces a further reduction in state separation. Several states of the anion lie less than 100 kcal/mol above the ground state. This anion, which has the same type of geometry as formaldehyde (*vide infra*), has two N lone pairs. The set of Lewis-type NBOs which best describes the ground state density hybridizes the two nitrogen lone pairs as a higher energy n_{2p_x} orbital and the other n_{2sp_y}; H_2CO similarly contains the same two lone pairs on O. NBO analysis of states involving excitation out of the lone pairs in both CH_2N^- and CH_2O show that the HOMO is primarily of $2p_x$ character, and more energy is needed to excite from the more stable lone pair MO which is of sp_y character. In CH_2NH and CH_2OH^+, the single lone pair is of sp_xp_y character, indicating that a rehybridization occurs upon protonation.

The greater contributions from the CH and NH bonds and antibonds in excited state $CH_2NH_2^+$ (Table III) leads to several states which break one or more of these bonds and dissociate.[50] The tenth singlet state breaks both C–H bonds in a symmetric manner, while the triplet dissociations break the symmetry by dissociating only one of two equivalent bonds. Several of the singlet states optimize to the same twisted C_{2d} geometry [Fig. 3(a)] due to significant MO mixing, while a reduced C_2 triplet excited state geometry with a

TABLE IV. Vertical excitation energies (kcal/mol), adiabatic excitation energies, optimized geometries, and changes in orbital occupancy for CH_2NH.

State	Symmetry	Transition	VEE	AEE	r_{CN}	r_{NH_5}	$\phi_{H_4CNH_3}$	$\phi_{H_5NCH_3}$	Population change[a]
Ground state									
0	$1\,^1A'$				1.2522	1.0052	0.00	0.00	
Singlet states									
1	$1\,^1A''$	$n_{N(2p_{xy})} \to \pi^*_{CN}$	135.9	94.2	1.3165	1.0092	25.98	77.01	$\Delta\rho(\pi^*)=+0.927$
2	$2\,^1A'$	$n_{N(2p_{xy})} \to r_{C(3sp_y)}/r_{N(3s)}/\sigma^*_{NH}$	192.2	175.1	1.2038	1.0540	0.00	0.00	
3	$3\,^1A'$	$\pi_{CN} \to \pi^*_{CN}$	206.7	178.8	1.5420	1.0223	45.29	48.36	$\Delta\rho(\pi)=-0.802$
									$\Delta\rho(\pi^*)=+0.912$
4	$2\,^1A''$	$\pi_{CN} \to r_{N(3sp_x)}/r_{C(3sp_{xy})}/\sigma^*_{NH}$	209.7	200.3	1.3548	1.0500	0.00	0.00	$\Delta\rho(\pi)=-0.993$
5	$4\,^1A'$	$n_{N(2p_{xy})} \to r_{C(3sp_y)}$	220.6	197.0	1.1931	1.0495	0.00	0.00	
7	$3\,^1A''$	$\pi_{CN} \to r_{C(3sp_{xy})}/r_{H_3(2s)}/\sigma^*_{CH_3}$	233.8	208.0	1.2802	1.0216	0.00	38.37	$\Delta\rho(\pi)=-0.735$
8	$4\,^1A''$	$n_{N(2p_{xy})} \to r_{C(3p_z)}/r_{N(3p_z)}$	235.6	215.4	1.1862	1.0005	1.33	30.23	$\Delta\rho(r_c)=+0.574$
									$\Delta\rho(r_N)=+0.225$
10	$6\,^1A''$	$\sigma_{CH_3}/\sigma_{CN}/\pi_{CN}/\sigma_{NH} \to \pi^*_{CN}$	241.9	94.2	1.3165	1.0092	25.98	77.01	$\Delta\rho(\pi)=-0.242$
									$\Delta\rho(\pi^*)=+0.667$
Triplet states									
1	$1\,^3A'$	$\pi_{CN} \to \pi^*_{CN}$	99.7	63.3	1.4228	1.0119	42.32	76.56	$\Delta\rho(\pi)=-0.994$
									$\Delta\rho(\pi^*)=+0.988$
2	$1\,^3A''$	$n_{N(2p_{xy})} \to \pi^*_{CN}$	109.5	62.8	1.4118	1.0099	44.92	30.50	$\Delta\rho(\pi^*)=+0.959$
3	$2\,^3A'$	$n_{N(2p_{xy})} \to \sigma^*_{NH}/r_{C(3s)}/r_{N(3s)}$	181.4	63.3	1.4228	1.0119	42.32	76.56	
4	$2\,^3A''$	$\pi_{CN} \to r_{C(3s)}/r_{N(3s)}/\sigma^*_{NH}$	202.6		Dissociative—N–H bond broken				
5	$3\,^3A'$	$n_{N(2p_{xy})}/\sigma_{CH}(2) \to r_{C(3sp_{xy})}/\sigma^*_{CH_3}/\sigma^*_{NH}/r_{H_3(2s)}$	210.6		Dissociative—C–H_3 bond broken				
7	$3\,^3A''$	$\pi_{CN}/\sigma_{CH_3}/\sigma_{CN}/\sigma_{NH} \to \pi^*_{CN}$	219.9	62.8	1.4118	1.0099	44.92	30.50	
8	$4\,^3A''$	$\pi_{CN} \to r_{C(3p_{xy})}/\sigma^*_{CH_3}/r_{H_3(2s)}$	230.5	63.3	1.4228	1.0119	42.32	76.56	
10	$6\,^3A''$	$\pi_{CN} \to r_{C(3p_{xy})}/\pi^*_{CN}/r_{C(3p_z)}$	238.1	63.3	1.4228	1.0119	42.32	76.56	

[a]Change(s) in π, $\pi*$, or $r_{(3p_z)}$ orbital occupancies for states in which they are the major contributors.

significantly longer CN bond (1.366 Å) and a CH_2 group pyramidalized 48° out of plane [Fig. 3(c)] appears to be the most stable configuration. In general, higher energy cation Rydberg transitions collapse to the adiabatic geometry of a lower valence excited state.
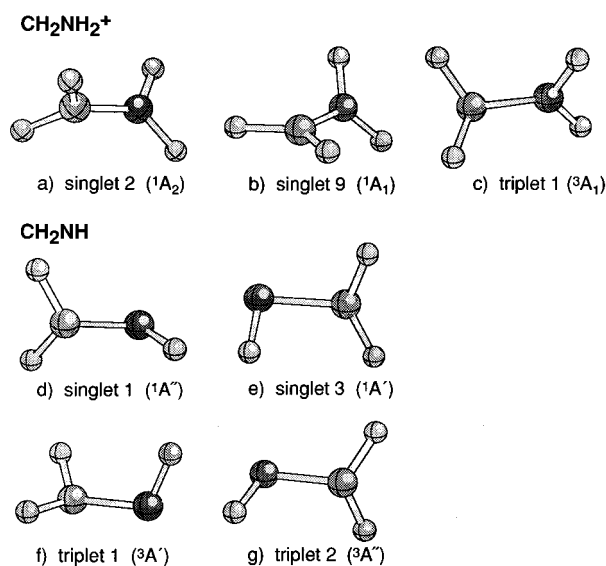
CH2NH2+

a) singlet 2 ($^1A_2$)   b) singlet 9 ($^1A_1$)   c) triplet 1 ($^3A_1$)

CH2NH

d) singlet 1 ($^1A''$)   e) singlet 3 ($^1A'$)

f) triplet 1 ($^3A'$)   g) triplet 2 ($^3A''$)

FIG. 3. Nonplanar excited state optimized geometries (CIS 6-31+G*) of $CH_2NH_2^+$ and CH_2NH.

The degree of nonplanarity of the adiabatic excited state geometries of CH_2NH is described by the dihedral angles in the second and third last columns of Table IV. When the CN bond is weakened by excitation out of the π bond or into the π^* antibond, the NH bond twists out of the plane and the CH_2 group pyramidalizes, either in the opposite direction [Figs. 3(d) and 3(g)] or in the same direction [Figs. 3(e) and 3(f)]. The correlation between π, π^*, or r_{3p_z} character and the amount of nonplanar distortion can be seen by comparing the two torsion angles with the change in population of the π, π^*, or the sum of the $r_{C(3p_z)}$ and $r_{N(3p_z)}$ populations in the last column of Table IV. For nonplanar geometries this change is at least 0.7 e. An exception is the fourth singlet state, in which the planar geometry appears to be stabilized by partial population of the σ^*_{NH} orbital. For the other states, the greater this change in population, the larger the nonplanar distortion.

Comparison of the excited state optimized geometries of CH_2N^- (Table V) and CH_2O shows that the CH_2N^- overall negative charge stabilizes the planar geometries relative to nonplanar distortions such that only the triplet $n_{N(2p_x)} \to \pi^*$ excitation causes the CH bonds to bend out of the plane. Because of the higher energy of the CH_2N^- HOMO, which is primarily the $n_{N(2p_x)}$ lone pair, compared to that of CH_2O, which also includes some σ_{CH} and π_{CO} character with the $n_{O(2p_x)}$ orbital, an electron is more easily excited from this orbital (Table V).

TABLE V. Vertical excitation energies (kcal/mol), adiabatic excitation energies, and optimized geometries for CH_2N^-.

State	Symmetry	Transition	VEE	AEE	r_{CN}	r_{CH}	θ_{NCH}
Ground state							
0	$1\,^1A_1$				1.2406	1.1229	125.28
Singlet states							
1	$1\,^1A_2$	$n_{N(2p_x)} \rightarrow \pi^*_{CN}/r_{C(3p_z)}$	60.1	55.4	1.3203	1.0863	121.47
2	$1\,^1B_2$	$n_{N(2p_x)} \rightarrow r_{C(3s)}/r_{N(3sp_y)}$	76.5	73.7	1.1983	1.1013	123.83
3	$2\,^1B_2$	$n_{N(2p_x)} \rightarrow r_{C(3p_y)}$	91.2	88.9	1.1969	1.1127	126.48
4	$2\,^1A_1$	$n_{N(2p_x)} \rightarrow r_{C(3p_x)}$	97.8	94.1	1.2001	1.0946	121.75
5	$2\,^1A_2$	$n_{N(2p_x)} \rightarrow r_{C(3p_z)}/r_{N(3p_z)}$	114.9	113.8	1.2214	1.1020	123.45
6	$1\,^1B_1$	$\pi_{CN} \rightarrow r_{C(3sp_x)}$	142.0	132.0	1.3506	1.0777	122.42
7	$3\,^1A_1$	$\pi_{CN}/n_{N(2p_x)} \rightarrow r_{C(3p_z)}/\pi^*_{CH}/r_{C(3p_x)}$	153.5	145.9	1.3401	1.0881	122.79
10	$3\,^1A_2$	$\pi_{CN} \rightarrow r_{C(3p_x)}/\pi^*_{CN}$	160.2	148.9	1.3540	1.0764	120.27
12	$3\,^1B_1$	$n_{N(2p_x)} \rightarrow \pi^*_{CN}/\sigma^*_{CN}/r_{C(3p_z)}$	180.7	160.6	1.4709	1.0734	115.07
14	$5\,^1A_1$	$\pi_{CN}/n_{N(2sp_y)} \rightarrow \pi^*_{CN}/r_{N(3p_z)}$	203.6	189.9	1.3921	1.0980	122.69
Triplet states							
1	$1\,^3A_2$	$n_{N(2p_x)} \rightarrow \pi^*_{CN}/r_{C(3p_z)}$	42.8	31.4	1.3718	1.0976	113.11
2	$1\,^3B_2$	$n_{N(2p_x)} \rightarrow r_{C(3s)}/r_{N(3sp_y)}$	71.6	68.8	1.1950	1.1070	124.18
3	$2\,^3B_2$	$n_{N(2p_x)} \rightarrow r_{C(3p_y)}$	85.1	82.7	1.1963	1.1210	127.21
4	$1\,^3A_1$	$n_{N(2p_x)}/\sigma_{CH}(2) \rightarrow \pi^*_{CN}$	92.3	88.1	1.1897	1.1078	122.16
5	$2\,^3A_1$	$\pi_{CN} \rightarrow \pi^*_{CN}$	100.2	77.1	1.4358	1.0981	124.04
6	$2\,^3A_2$	$n_{N(2p_x)} \rightarrow r_{C(3p_z)}/\pi^*_{CN}/r_{N(3p_z)}$	112.1	110.6	1.2134	1.1019	123.56
7	$1\,^3B_1$	$\pi_{CN} \rightarrow r_{C(3s)}$	135.6	123.9	1.3722	1.0794	120.90
8	$2\,^3B_1$	$n_{N(2p_x)} \rightarrow \pi^*_{CN}$	144.5	128.0	1.3922	1.0755	119.92
11	$3\,^3B_1$	$\pi_{CN} \rightarrow r_{C(3p_y)}/r_{N(3s)}$	153.7	141.6	1.3697	1.0818	122.93
13	$3\,^3A_2$	$\pi_{CN} \rightarrow r_{C(3p_x)}/\pi^*_{CN}$	158.0	146.7	1.3553	1.0778	120.27

[a] $\phi_{HCNH} = 53.95°$.

TABLE VI. Vertical excitation energies (kcal/mol), natural charge shifts, adiabatic excitation energies, and optimized geometries for CH_2OH^+.

State	Symmetry	Transition	VEE	Δq_C	Δq_O	AEE	r_{CO}	r_{OH_5}	θ_{COH_5}
Ground state									
0	$2\,^1A''$						1.2317	0.9600	117.75
Singlet states									
1[a]	$1\,^1A''$	$\pi_{CO}/\sigma_{CH}(2)/\sigma_{OH} \rightarrow \pi^*_{CO}$	164.6	−0.525	+0.154	131.5	1.2540	0.9685	119.09
2	$2\,^1A''$	$\sigma_{CO}/\sigma_{CH_3}/\pi_{CO} \rightarrow \sigma^*_{CO}/n_{C(2p_{xy})}$	256.0	−0.430	+0.257	Unresolvable curve crossing			
3[a]	$2\,^1A'$	$\pi_{CO} \rightarrow \pi^*_{CO}$	260.8	−0.383	+0.408	131.5	1.2540	0.9685	119.09
4	$3\,^1A'$	$n_O/\sigma_{CH}(2) \rightarrow \sigma^*_{OH}/r_{C(3p_y)}/r_{O(3s)}$	297.1	−0.130	+0.240	Dissociative—O–H bond broken			
5[a]	$3\,^1A''$	$\pi_{CO}/\sigma_{OH}/\sigma_{CH_4} \rightarrow \pi^*_{CO}$	312.8	−0.420	+0.266	131.5	1.2540	0.9685	119.09
6	$4\,^1A''$	$\pi_{CO} \rightarrow \sigma^*_{OH}/\pi^*_{CO}/r_{H_5}$	321.8	−0.040	+0.503	Dissociative—O–H bond broken			
7	$4\,^1A'$	$\pi_{CO}/\sigma_{CH}(2)/\sigma_{OH}/n_O \rightarrow \pi^*_{CO}/r_{C(3sp_y)}/\sigma_{CH}$	336.6	−0.186	+0.152	Dissociative—C–H bonds broken			
8[a]	$5\,^1A''$	$\sigma_{CH_4}/n_O \rightarrow r_{C(3p_{xy})}/\pi^*_{CO}/r_{O(3sp_x)}$	353.2	−0.354	+0.156	131.5	1.2540	0.9685	119.09
Triplet states									
1[b]	$1\,^3A''$	$\pi_{CO}/\sigma_{CH_4}/\sigma_{CH_3}/\sigma_{OH} \rightarrow \pi^*_{CO}$	141.8	−0.524	+0.126	108.3	1.2538	0.9631	118.59
2[b]	$1\,^3A'$	$\pi_{CO} \rightarrow \pi^*_{CO}$	161.4	−0.738	+0.764	108.3	1.2538	0.9631	118.59
3	$2\,^3A''$	$\sigma_{CO}/\sigma_{CH_3} \rightarrow \sigma^*_{CO}/\sigma^*_{CH_3}$	227.7	−0.432	+0.202	Dissociative—C–H_3 bond broken			
4	$2\,^3A'$	$\sigma_{OH}/\sigma_{CH_4}/n_O/\sigma_{CH_3} \rightarrow \sigma^*_{OH}/\sigma^*_{CH_4}$	274.3	−0.055	+0.303	Dissociative—O–H bond broken			
5	$3\,^3A''$	$\pi_{CO}/\sigma_{CH_4}/\sigma_{OH} \rightarrow \pi^*_{CO}/\sigma^*_{CH_4}$	279.6	−0.414	+0.188	Dissociative—C–H_4 bond broken			
6	$4\,^3A''$	$\pi_{CO} \rightarrow \sigma^*_{OH}/r_{H_5(2s)}$	303.1	+0.102	+0.115	Dissociative—O–H bond broken			
7	$3\,^3A'$	$\sigma_{CH}(2)/\sigma_{OH}/n_O \rightarrow \sigma^*_{CH}/\sigma^*_{OH}/r_{H_3(2s)}$	305.0	−0.009	+0.537	Dissociative—O–H bond broken			
8	$4\,^3A'$	$\sigma_{CH}(2)/n_O/\sigma_{OH} \rightarrow \sigma^*_{CH_4}/r_{C(3sp_y)}/\sigma^*_{CH_3}$	320.9	−0.008	+0.047	Dissociative—C–H_4 bond broken			

[a] $\phi_{H_4COH_3} = 52.06°$ (pyramidal distortion angle), H_5 opposite (180° from) bisector of HCH angle.
[b] $\phi_{H_4OCH_3} = 75.02°$, H_5 opposite bisector of HCH angle.

TABLE VII. Vertical excitation energies (kcal/mol), adiabatic excitation energies, and optimized geometries for formaldehyde.

State	Symmetry	Transition	VEE[a]	Hadad[b]	AEE	r_{CO}	r_{CH}	θ_{OCH}	ϕ_{HCOH}
Ground state									
0	$2\,^1A_1$					1.1862	1.0923	121.83	0.00
Singlet states									
1	$1\,^1A_2$	$n_{O(2p_x)} \rightarrow \pi^*_{CO}$	108.2	105.6	103.5	1.2552	1.0856	118.01	26.10
2	$1\,^1B_2$	$n_{O(2p_x)}/\sigma_{CH}(2) \rightarrow r_{C(3s)}/\sigma^*_{CH}(2)$	203.3	158.0	197.8	1.1311	1.1842	130.73	0.00
3	$2\,^1B_2$	$n_{O(2p_x)}/\sigma_{CH}(2) \rightarrow r_{C(3p_y)}/\sigma^*_{CO}$	219.3	176.6	214.5	1.1441	1.1452	127.86	0.00
4	$2\,^1A_1$	$n_{O(2p_x)}/\sigma_{CH}(2) \rightarrow r_{C(3p_z)}$	227.5	195.3	186.4	1.4889	1.0774	107.97	44.72
5	$1\,^1B_1$	$\pi_{CO}/n_{O(2sp_y)} \rightarrow \pi^*_{CO}/\sigma^*_{CO}$	234.2	229.9	186.4	1.4889	1.0774	107.97	44.72
6	$3\,^1A_1$	$\pi_{CO}/n_{O(2sp_y)} \rightarrow \pi^*_{CO}$	235.4	211.9	186.4	1.4889	1.0774	107.97	44.72
8	$3\,^1A_2$	$\sigma_{CH}(2)/n_{O(2p_x)} \rightarrow \pi^*_{CO}$	269.9	232.4	214.5	1.1441	1.1452	127.86	0.00
9	$2\,^1B_1$	$\pi_{CO} \rightarrow r_{C(3s)}/r_{O(3s)}$	270.0	250.0	254.4	1.3131	1.0767	116.98	0.00
Triplet states									
1	$1\,^3A_2$	$n_{O(2p_x)} \rightarrow \pi^*_{CO}$	89.8	95.7	82.8	1.2552	1.0926	114.26	47.42
2	$1\,^3A_1$	$\pi_{CO} \rightarrow \pi^*_{CO}$	120.9	155.0	82.5	1.4080	1.0726	113.24	40.00
3	$1\,^3B_2$	$n_{O(2p_x)}/\sigma_{CH}(2) \rightarrow r_{C(3s)}/\sigma^*_{CH}(2)$	193.8	160.7	82.8	1.2552	1.0926	114.26	47.42
4	$1\,^3B_1$	$n_{O(2sp_y)} \rightarrow \pi^*_{CO}$	203.9	211.7	164.3	1.4681	1.0731	105.89	37.01
5	$2\,^3B_2$	$n_{O(2p_x)}/\sigma_{CH}(2) \rightarrow r_{C(3p_y)}/r_{O(3s)}/\sigma^*_{CO}$	211.0	178.7	206.9	1.1504	1.1368	127.55	0.00
6	$2\,^3A_1$	$n_{O(2p_x)}/\sigma_{CH}(2) \rightarrow r_{C(3p_x)}$	218.6	179.4	211.3	1.1385	1.2027	124.02	0.00
8	$3\,^3A_2$	$\sigma_{CH}(2)/n_{O(2p_x)} \rightarrow \pi^*_{CO}$	249.2	242.6	218.1	1.2926	1.1601	132.00	28.56
10	$2\,^3B_2$	$n_{O(2p_x)}/\sigma_{CH}(2) \rightarrow \pi^*_{CO}/r_{C(3sp_y)}/\sigma^*_{CH}(2)$	273.1		237.8	1.1444	1.2144	111.39	0.00

[a]This work.
[b]Reference 10, CIS-MP2/6-311(2+,2+)G**.

TABLE VIII. Vertical excitation energies (kcal/mol), adiabatic excitation energies, and optimized geometries for HCO^-.

State	Symmetry	Transition	VEE	AEE	r_{CO}	r_{CH}	θ_{HCO}
Ground state							
0	$2\,^1A'$				1.2241	1.1895	109.33
Singlet states							
1	$1\,^1A''$	$n_{C(2sp_{xz})}/n_{O(2p_{xz})} \rightarrow \pi^*_{CO}/\sigma^*_{CH}/r_{C(3p_z)}$	53.3	47.4	1.2175	1.1102	128.49
2	$2\,^1A'$	$n_{C(2sp_{xy})}/n_{O(2p_x)} \rightarrow r_{C(3p_x)}/\sigma^*_{CH}$	71.7	60.8	1.1590	1.0983	125.76
3	$3\,^1A'$	$n_{C(2sp_{xy})}/n_{O(2p_x)} \rightarrow \sigma^*_{CO}/\sigma^*_{CH}$	84.6	73.7	1.1590	1.1300	128.16
4	$2\,^1A''$	$n_{C(2sp_{xy})}/n_{O(2p_x)} \rightarrow r_{C(3p_z)}/\sigma^*_{CO}$	107.9	99.9	1.1864	1.1078	127.87
5	$4\,^1A'$	$n_{C(2sp_{xy})}/n_{O(2p_x)}/\sigma_{CH} \rightarrow r_{C(3p_x)}$	110.3	105.8	1.1711	1.1666	117.44
6	$3\,^1A''$	$n_{C(2sp_{xy})}/n_{O(2p_x)} \rightarrow \pi^*_{CO}/r_{C(3p_z)}$	182.5	159.2	1.4113	1.1230	102.94
7	$5\,^1A'$	$n_{O(2p_x)}/n_{C(2sp_{xy})}/\sigma_{CH} \rightarrow r_{O(3p_y)}/r_{C(3sp_y)}$	187.6	181.3	1.1554	1.1315	122.37
8	$6\,^1A'$	$\pi_{CO}/n_{O(2p_x)}/n_{C(2sp_{xy})}/\sigma_{CH} \rightarrow r_{C(3p_x)}/\pi^*_{CO}/r_{C(3p_z)}$	202.9	180.2	1.4716	1.1104	102.42
9	$4\,^1A''$	$\pi_{CO} \rightarrow r_{C(3sp_y)}/r_{O(3s)}$	206.5	187.8	1.3770	1.0931	103.47
10	$7\,^1A'$	$\pi_{CO}/n_{C(2p_{xy})}/\sigma_{CH} \rightarrow \pi^*_{CO}/r_{O(3p_z)}/r_{C(3p_z)}$	210.7	210.2	1.2124	1.1571	112.55
15	$6\,^1A''$	$\sigma_{CO}/\sigma_{CH}/\pi_{CO}/n_{O(2p_x)} \rightarrow \pi^*_{CO}$	238.9	197.8	1.4747	1.1524	99.95
Triplet states							
1	$1\,^3A''$	$n_{C(2sp_{xz})}/n_{O(2p_{xz})} \rightarrow \pi^*_{CO}/\sigma^*_{CO}$	27.6	20.6	1.2461	1.1044	125.86
2	$1\,^3A'$	$n_{C(2sp_{xy})}/n_{O(2p_x)} \rightarrow r_{C(3s)}/\sigma^*_{CH}$	60.6	48.8	1.1554	1.1144	128.08
3	$2\,^3A'$	$n_{C(2sp_{xz})}/n_{O(2p_{xz})} \rightarrow r_{C(3p_y)}/\sigma^*_{CH}$	76.3	63.1	1.1491	1.1187	129.97
4	$3\,^3A'$	$n_{C(2sp_{xy})}/n_{O(2p_x)} \rightarrow r_{C(3p_y)}/r_{O(3s)}/\sigma^*_{CH}$	80.1	68.3	1.1556	1.1249	129.25
5	$2\,^3A''$	$n_{C(2sp_{xz})}/n_{O(2p_{xz})} \rightarrow \sigma^*_{CH}/\pi^*_{CO}$	96.3	87.8	1.1760	1.1184	126.33
6	$4\,^3A'$	$\pi_{CO} \rightarrow \pi^*_{CO}$	134.9	102.1	1.4422	1.1149	101.87
7	$3\,^3A''$	$n_{C(2sp_{xy})}/n_{O(2p_x)} \rightarrow \pi^*_{CO}$	158.4	141.3	1.3454	1.1268	101.55
8	$5\,^3A'$	$n_{C(2sp_{xy})}/n_{O(2p_x)} \rightarrow r_{C(3sp_{xy})}/r_{O(3p_y)}/\sigma^*_{CH}$	163.9		Dissociative—C–H bond broken		
9	$6\,^3A'$	$n_{C(2sp_{xy})}/n_{O(2p_x)}/\sigma_{CH} \rightarrow r_{O(3p_y)}/\sigma^*_{CH}/r_{C(3sp_{xy})}$	191.2		Dissociative—C–H bond broken		
10	$7\,^3A'$	$n_{O(2p_x)}/n_{C(2sp_{xy})}/\sigma_{CH} \rightarrow r_{C(3p_x)}/r_{O(3p_x)}$	197.5	191.6	1.1566	1.1376	115.68
11	$4\,^3A''$	$\pi_{CO}/\sigma_{CH} \rightarrow \pi^*_{CO}/r_{C(3sp_y)}/r_{O(3s)}$	199.5	181.2	1.3837	1.0948	103.24
14	$6\,^3A''$	$n_{O(2p_{xy})}/n_{C(2sp_{xy})}/\sigma_{CH} \rightarrow \pi^*_{CO}/r_{O(3p_z)}$	224.5	221.9	1.2563	1.1364	112.23

CH$_2$OH$^+$

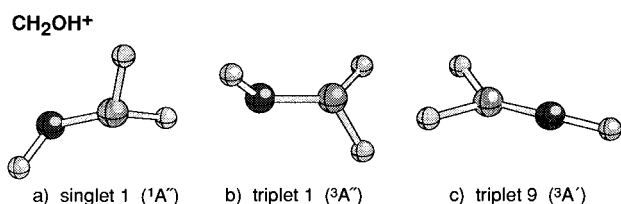a) singlet 1 ($^1A''$)   b) triplet 1 ($^3A''$)   c) triplet 9 ($^3A'$)

FIG. 4. Nonplanar excited state optimized geometries (CIS 6-31+G*) of CH$_2$OH$^+$.

C. Formaldehyde

The excited states of protonated formaldehyde, CH$_2$OH$^+$, are listed in Table VI. Over the series CH$_2$CH$^-$, CH$_2$NH, CH$_2$OH$^+$, as the electronegativity difference between C and its partner atom increases, and the overall charge of the species becomes more positive, the states become more widely separated. The greater shift in charge toward the carbon atom upon excitation in the molecules with more polar CX bonds is due to two factors. The first is the transfer of more density from orbitals centered on X$_2$ (n_{X_1}) to Rydbergs on C$_1$ as the X atom becomes more electronegative.[51] The second factor is the increased polarization of the π bond toward X$_2$ and π^* toward C$_1$ as X$_2$ becomes more electronegative.[52]

Table VII lists the excited state assignments and vertical transition energies of CH$_2$O, along with the CIS-MP2/6-311(2+,2+)G** results of Hadad *et al.*[14] Most of the assignments and valence state energies agree fairly well, but their CIS-MP2 Rydberg excitation energies are lower due to the effect of electron correlation. Two lone pairs on the same atom remain distinct from each other, hybridized $2p_x$ and $2sp_y$. However, when two lone pairs are on adjacent heavy atoms, as in HCO$^-$ (Table VIII), the excitations become noticeably more delocalized. It also takes much less energy to excite an electron out of the HOMO, which is a combination of the C and O lone pairs (more out of the less stable n_C lone pair than n_O). Following the series CH$_2$CH$^-$, CH$_2$N$^-$, HCO$^-$, one sees the first singlet and triplet energies diminish as the species maintains a negative charge but hydrogens are lost.

Table VI shows even more curve crossing and dissociation for excited CH$_2$OH$^+$ than for CH$_2$NH$_2^+$. The shift in density away from the oxygen toward carbon upon excitation into the σ^*_{OH} antibond weakens the OH bond. The most

TABLE IX. Excited state deprotonation energies (kcal/mol) for CH$_2$CH$_2$.

Deprotonation reaction[a]	Transition[b]	Vertical deprotonation energy[c]	Adiabatic deprotonation energy
Ground state			
CH$_2$CH$_2$(0)$\rightarrow$CH$_2$CH$^-$(0)+H$^+$	$\cdots$	422.6	422.6
Singlet states			
CH$_2$CH$_2$(2)$\rightarrow$CH$_2$CH$^-$(12)+H$^+$	$\pi_{CC}/[n_C]\rightarrow\pi^*_{CC}/r_{C(3p_z)}$	401.4	452.5
$^1B_{1u}$ $^1A''$			
CH$_2$CH$_2$(3)$\rightarrow$CH$_2$CH$^-$(7)+H$^+$	$\pi_{CC}\rightarrow r_{C(3p_x)}$	364.3	340.9
$^1B_{1g}$ $^1A'$			
CH$_2$CH$_2$(4)$\rightarrow$CH$_2$CH$^-$(13)+H$^+$	$\pi_{CC}\rightarrow r_{C(3p_y)}$	396.2	398.0
$^1B_{2g}$ $^1A''$			
CH$_2$CH$_2$(5)$\rightarrow$CH$_2$CH$^-$(11)+H$^+$	$\pi_{CC}/[n_{CC}]\rightarrow r_{C(3p_z)}/\pi^*_{CC}$	363.4	366.7
^1A_g $^1A'$			
CH$_2$CH$_2$(9)$\rightarrow$CH$_2$CH$^-$(17)+H$^+$	$\sigma_{CC}/\sigma_{CH}\rightarrow\pi^*_{CC}$	391.8	292.1
$^1B_{2g}$ $^1A''$			
Triplet states			
CH$_2$CH$_2$(1)$\rightarrow$CH$_2$CH$^-$(3)+H$^+$	$\pi_{CC}\rightarrow\pi^*_{CC}$	425.4	414.1
$^3B_{1u}$ $^3A''$			
CH$_2$CH$_2$(3)$\rightarrow$CH$_2$CH$^-$(9)+H$^+$	$\pi_{CC}\rightarrow r_{C(3p_x)}$	363.4	338.7
$^3B_{1g}$ $^3A'$			
CH$_2$CH$_2$(4)$\rightarrow$CH$_2$CH$^-$(6)+H$^+$	$\pi_{CC}\rightarrow r_{C(3p_y)}$	342.5	326.1
$^3B_{2g}$ $^3A''$			
CH$_2$CH$_2$(5)$\rightarrow$CH$_2$CH$^-$(8)+H$^+$	$\pi_{CC}\rightarrow r_{C(3p_z)}/\pi^*_{CC}$	358.1	358.9
^3A_g $^3A'$			
CH$_2$CH$_2$(9)$\rightarrow$CH$_2$CH$^-$(18)+H$^+$	$\sigma_{CC}/\sigma_{CH}\rightarrow\pi^*_{CC}$	393.9	337.5
$^3B_{2g}$ $^3A''$			

[a]Numbers in parentheses refer to states numbered in earlier tables.
[b]Orbitals in brackets make a minor contribution to the excitation in one species, and none in the other.
[c]Difference in vertical excitation energies (no geometric relaxation).

stable excited state geometries have the OH bond 180° opposite the bisector of the HCH angle [Figs. 4(a) and 4(b)]. The ninth triplet state relieves strain by linearizing the COH angle.

The correlation of π/π^* character and CO bond lengthening and nonplanarity for the excited states of CH_2O can be seen in Table VII. The CO bond length increases by 0.3 Å for the formaldehyde adiabatic $\pi \rightarrow \pi^*$ singlet state, the HCH angle opens up by 27°, and the geometry distorts to a nonplanar structure. This contrasts with the structure found by Hadad et al.,[14] which had similar bond lengths and angles, but was planar. The $\pi \rightarrow \pi^*$ triplet state CO bond lengthens by a lesser amount. The CO bond lengths for $n_O \rightarrow \pi^*$ states increase slightly, but the structure is even more pyramidal.

The optimized geometries of CH_2O states exciting out of MO 8 (the HOMO) composed of $n_{O(2p_x)}/\sigma_{CH}(2)$ have shorter CO bond lengths. Depopulation of the oxygen lone pair decreases the diffuseness of the density around oxygen and moves electrons toward the CO σ bond to strengthen it, confirmed by contour plots of these orbitals. These results are consistent with the CIS optimized structures calculated by Hadad et al.[14] for the states labeled $n_y \rightarrow 3s(1\ ^1B_2)$ and $n_y \rightarrow 3p_z(2\ ^1B_2)$, which were planar with shorter CO bond lengths and smaller HCH angles. This effect is also seen in HCO^- (Table VIII). In this species, the HOMO is a mixture of the carbon and oxygen lone pairs, with the less stable carbon lone pair more easily depopulated. Thus even the excitations of mostly $n_{O(2p_x)}$ character, similar to those in formaldehyde, also depopulate the adjacent $n_{C(2px_y)}$ NBO. In fact, if enough density is removed from the valence region to Rydberg orbitals, the two adjacent C and O $2p_{xy}$ lone pairs, each left with only 1.2–1.5 e, are better described as a third CO bond of both σ and π character with occupancy of nearly 2.0 coupled with a less populated σ^*/π^* orbital. This increased bonding causes the shorter bond length, and is accompanied by an increase in the HCO angles.

IV. EXCITED STATE DEPROTONATION ENERGIES

For each acid-base pair, the energy difference between ground state optimized minima of the protonated acid BH^+ and deprotonated base B is the ground state deprotonation energy, or electronic contribution to the proton affinity

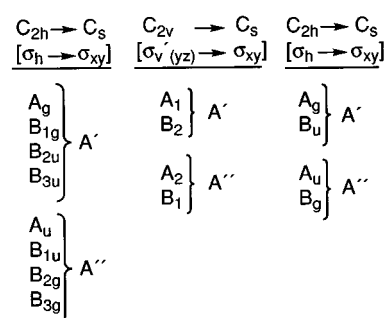$$\Delta E_0(BH^+) = -E_0(BH^+) + E_0(B). \quad (1)$$

The base B may be an anion. This value differs from the experimental proton affinity by the vibrational, rotational, and translational contributions. These factors are generally found to decrease the calculated deprotonation energies by a few kcal/mol due to partial cancellation between protonated and deprotonated species.[19]

For CH_2CH_2 we obtained a ground state deprotonation energy of 422.6 kcal/mol, which is consistent with previous calculated values of 418–424 kcal/mol (Ref. 19) and higher than the experimental result of 406.0 kcal/mol.[53] The protonation energy of ground state CH_2NH at the HF/6-31 $+G(d,p)$ level, 222.90 kcal/mol, is higher than the MP2/6-31$+G^*(d,p)$ value of 216.8 kcal/mol (Ref. 23) and

other calculated values in the range of 200–208 kcal/mol at 298 K using various ab initio methods.[23,29] The experimental proton affinity[54] of CH_2NH is 204.1 kcal/mol.

The deprotonation energy of CH_2OH^+ at the HF/6-31 $+G(d,p)$ level, 184.4 kcal/mol, confirms the value at the same level of theory obtained by Del Bene,[23] and is higher than the MP2/6-31$+G(d,p)$ value of 176.6 kcal/mol, as well as the G2 value,[28] 168.7 kcal/mol. Calculations of the CH_2O proton affinity are in the range of 167–179 kcal/mol for a variety of different approaches.[20,21,23–27,55] These values are all within a few kcal/mol of the experimental value,[56] 171.7 kcal/mol. Correlation decreases the deprotonation energy by 6–8 kcal/mol, and the change in zero point and vibrational energy decreases the proton affinity by 6–10 kcal/mol. Our deprotonation energies are close to those from previous calculations, and can be compared with those of the species in their excited states.

The excited state protonations which we consider are those which preserve the symmetry, character and, if possible, geometry of the state. Planar symmetry groups[57] with some common symmetry elements can be mapped onto one another, as shown in Chart 1.

$$
\begin{array}{lll}
C_{2h} \rightarrow C_s & C_{2v} \rightarrow C_s & C_{2h} \rightarrow C_s \\
[\sigma_h \rightarrow \sigma_{xy}] & [\sigma_v'(yz) \rightarrow \sigma_{xy}] & [\sigma_h \rightarrow \sigma_{xy}]
\end{array}
$$

Excited state NBO analysis can be used as a helpful tool to "match" states of similar character (quantitatively similar depopulation and population of orbitals of the same type for both species) and compatible symmetry between the protonated and unprotonated species. The excited state adiabatic deprotonation energy may be written as

$$\Delta E_k^A(BH^+) = -E_i(BH^+) + E_j(B) = \Delta E_0(BH^+)$$
$$+ [-E_i^A(BH^+) + E_j^A(B)], \quad (2)$$

where k is an index for excited state matches $i-j$ for which a deprotonation energy can be determined, i is the excited state of protonated BH^+, j is the excited state of base B. $E_i^A(BH^+)$ and $E_j^A(B)$ are the adiabatic transition energies after the geometries of BH^+ and B have been optimized for states i and j, respectively. A corresponding "vertical deprotonation energy" (VDE) can be calculated from the vertical transition energies, $E_i^V(BH^+)$ and $E_j^V(B)$. This quantity shows the effect of electronic excitation independent of geometry relaxation.

Tables IX–XIII tabulate several vertical and adiabatic excited state deprotonation energies, ordered by the acid excited state, for the systems considered in this study, along with the ground state DE. Cations require much less energy to deprotonate; the ground state DE of $CH_2NH_2^+$ is a little

TABLE X. Excited state deprotonation energies (kcal/mol) for $CH_2NH_2^+$.

Deprotonation reaction	Transition	Vertical deprotonation energy	Adiabatic deprotonation energy
Ground state $CH_2NH_2^+(0) \rightarrow CH_2NH(0) + H^+$	...	222.9	222.9
Singlet states $CH_2NH_2^+(2) \rightarrow CH_2NH(3) + H^+$ $^1A_1$ $^1A'$	$\pi_{CN}/[n_N] \rightarrow \pi_{CN}^*$	195.2	286.8
$CH_2NH_2^+(3) \rightarrow CH_2NH(10) + H^+$ $^1B_1$ $^1A''$	$\sigma_{CN}/\sigma_{CH}/\pi_{CN} \rightarrow \pi_{CN}^*$	193.6	202.3
$CH_2NH_2^+(4) \rightarrow CH_2NH(4) + H^+$ $^1B_1$ $^1A''$	$\pi_{CN} \rightarrow r_{N(3sp_x)}/r_{C(3sp_x)}/\sigma_{NH}^*$	154.0	308.4
$CH_2NH_2^+(7) \rightarrow CH_2NH(7) + H^+$ $^1B_1$ $^1A''$	$\pi_{CN} \rightarrow r_{C(3sp_y)}/[r_{N(3sp_y)}]/\sigma_{CH}^*$	129.2	316.1
$CH_2NH_2^+(9) \rightarrow CH_2NH(11) + H^+$ $^1A_1$ $^1A'$	$\pi_{CN} \rightarrow \pi_{CN}^*/r_{N(3p_z)}/r_{C(3p_z)}$	137.9	124.3
Triplet states $CH_2NH_2^+(1) \rightarrow CH_2NH(1) + H^+$ $^3A_1$ $^1A'$	$\pi_{CN} \rightarrow \pi_{CN}^*$	198.4	194.0
$CH_2NH_2^+(3) \rightarrow CH_2NH(7) + H^+$ $^3B_1$ $^1A''$	$\pi_{CN}/\sigma_{CH}/\sigma_{CN} \rightarrow \pi_{CN}^*$	199.2	193.5
$CH_2NH_2^+(4) \rightarrow CH_2NH(4) + H^+$ $^3B_1$ $^1A''$	$\pi_{CN} \rightarrow \sigma_{NN}^*/r_{N(3s)}/r_{C(3s)}$	160.9	<0 (dissociative)
$CH_2NH_2^+(9) \rightarrow CH_2NH(8) + H^+$ $^3B_1$ $^1A''$	$\pi_{CN} \rightarrow r_{C(3sp_y)}/r_{N(3sp_y)}/\sigma_{CH}^*$	134.5	194.0

less than half of that of neutral ethylene. Each deprotonation reaction is labeled with the acid and base excited state and symmetry. Bracketed orbitals are those which make a minor contribution to the state of one species but not the other. For each reaction, the number of excited states that can be correlated between the protonated and deprotonated species indicates the similarity between the ground and excited state electronic structure of the two species. The CH_2CH_2/CH_2CH^- (Table IX), $CH_2NH_2^+/CH_2NH$ (Table X), and CH_2NH/CH_2N^- (Table XI) systems show a fairly high degree of correlation. CH_2NH and CH_2N^- have the most excited states with similar character. In both species the HOMO is primarily an in-plane nitrogen lone pair. Though this lone pair has slightly different hybridization, p_x for CH_2N^- and sp_xp_y CH_2NH, excitations from this orbital are distinct in both species. In contrast to the CH_2NH/CH_2N^- system, the CH_2OH^+/CH_2O system (Table XII), which nominally has the same bonding structure, shows much less correlation between the excited states. Only two singlet states and the relatively "pure" triplet $\pi \rightarrow \pi^*$ state have similar character. Few of the excited states of CH_2OH^+ are stable, and the excitations in both species are much more delocalized over the entire molecule. The HOMO is no longer primarily a single lone pair on one center, but extends into the σ_{CH} and σ_{OH} bonds.

We focus our attention first on the vertical deprotonation energies in order to understand the effects of electronic excitation in isolation from nuclear arrangements. The excited state VDEs are almost all lower than those of the ground state. For most excited states, this can be attributed to the consistently larger "gap" between the ground and first excited state and the lower density of states for the protonated species than the deprotonated one. Tables I–VIII show that the first vertical excitation energy decreases over the series: protonated cation>neutral species>deprotonated anion. Figure 5 compares the triplet vertical excitation energies of $CH_2NH_2^+$, CH_2NH, and CH_2N^-. The gap decreases over this series from 124.2 to 99.7 to 42.8 kcal/mol, and the same trend in VEEs is seen for many excited states of similar character, such as the $\pi \rightarrow r_{C(3sp_y)}/[r_{N(3sp_y)}/\sigma_{CH}^*]$ states, highlighted in Fig. 5.

One cause of the lowered DE in the excited state may be associated with the decreased charge on X_2 due to the charge shift toward C_1 upon excitation of the base species. The lowered negative charge leads to less electrostatic attraction between the proton and anion, and less energy is gained by protonation of N. However, due to the different number of hydrogens on the X_2 atom, the charge of this atom alone is not always a reliable indicator.

For each acid/base deprotonation pair, the vertical transition energies of the base are consistently closer together

TABLE XI. Excited state deprotonation energies (kcal/mol) for CH_2NH.

Deprotonation reaction	Transition	Vertical deprotonation energy	Adiabatic deprotonation energy
Ground state $CH_2NH(0) \rightarrow CH_2N^-(0) + H^+$	$\cdots$	404.6	404.6
Singlet states			
$CH_2NH(1) \rightarrow CH_2N^-(1) + H^+$ $^1A''$ $\quad$ $^1A_2$	$n_N \rightarrow \pi_{CN}^*$	328.8	365.8
$CH_2NH(2) \rightarrow CH_2N^-(2) + H^+$ $^1A'$ $\quad$ $^1B_2$	$n_N \rightarrow r_{C(3sp_y)}/r_{C(3sp_y)}$	288.9	303.2
$CH_2NH(3) \rightarrow CH_2N^-(7) + H^+$ $^1A'$ $\quad$ $^1A_1$	$\pi_{CN}/n_N \rightarrow \pi_{CN}^*/r_{C(3p_z)}$	351.4	371.8
$CH_2NH(4) \rightarrow CH_2N^-(6) + H^+$ $^1A''$ $\quad$ $^1B_1$	$\pi_{CN} \rightarrow r_{C(3sp_x)}/r_{N(3sp_x)}$	336.9	336.3
$CH_2NH(5) \rightarrow CH_2N^-(8) + H^+$ $^1A'$ $\quad$ $^1B_2$	$n_N \rightarrow r_{O(3sp_y)}$	340.6	353.9
$CH_2NH(11) \rightarrow CH_2N^-(14) + H^+$ $^1A'$ $\quad$ $^1A_1$	$\pi_{CN} \rightarrow \pi_{CN}^*/r_{C(3p_z)}/r_{N(3p_z)}$	352.8	374.8
Triplet states			
$CH_2NH(1) \rightarrow CH_2N^-(5) + H^+$ $^1A'$ $\quad$ $^3A_1$	$\pi_{CN} \rightarrow \pi_{CN}^*$	405.1	418.5
$CH_2NH(2) \rightarrow CH_2N^-(1) + H^+$ $^1A''$ $\quad$ $^3A_2$	$n_N \rightarrow \pi_{CN}^*/[r_{C(3p_z)}]$	337.9	373.2
$CH_2NH(3) \rightarrow CH_2N^-(2) + H^+$ $^1A'$ $\quad$ $^3B_2$	$n_N \rightarrow r_{C(3s)}/r_{N(3s)}$	294.8	410.2
$CH_2NH(4) \rightarrow CH_2N^-(7) + H^+$ $^1A''$ $\quad$ $^3B_1$	$\pi_{CN} \rightarrow r_{C(3s)}/r_{N(3s)}$	337.6	<0 (dissociative)
$CH_2NH(8) \rightarrow CH_2N^-(11) + H^+$ $^1A''$ $\quad$ $^3B_1$	$\pi_{CN} \rightarrow r_{O(3sp_y)}$	327.8	482.9
$CH_2NH(10) \rightarrow CH_2N^-(13) + H^+$ $^1A''$ $\quad$ $^3B_1$	$\pi_{CN} \rightarrow r_{C(3p_{xy})}/\pi_{CN}^*$	324.5	348.0

TABLE XII. Excited state deprotonation energies (kcal/mol) for CH_2OH^+.

Deprotonation reaction	Transition	Vertical deprotonation energy	Adiabatic deprotonation energy
Ground state $CH_2OH^+(0) \rightarrow CH_2O(0) + H^+$	$\cdots$	184.4	184.4
Singlet states			
$CH_2OH^+(3) \rightarrow CH_2O(6) + H^+$ $^1A_1$ $\quad$ $^1A'$	$\pi_{CO}/[n_O] \rightarrow \pi_{CO}^*$	159.0	239.2
$CH_2OH^+(8) \rightarrow CH_2O(8) + H^+$ $^1A_1$ $\quad$ $^1A'$	$\sigma_{CH}/n_O \rightarrow \pi_{CO}^*/[n_{C(3p_{xy})}/r_{O(3sp_x)}]$	101.1	267.4
Triplet states			
$CH_2OH^+(2) \rightarrow CH_2O(2) + H^+$ $^3A_1$ $\quad$ $^1A'$	$\pi_{CO} \rightarrow \pi_{CO}^*$	143.9	158.6

TABLE XIII. Excited state deprotonation energies (kcal/mol) for formaldehyde.

Deprotonation reaction	Transition	Vertical deprotonation energy	Adiabatic deprotonation energy
Ground state $CH_2O(0) \rightarrow HCO^-(0) + H^+$	$\cdots$	408.2	408.2
Singlet states $CH_2O(4) \rightarrow HCO^-(5) + H^+$ $^1A_1 \qquad ^1A'$	$n_{O(2p_x)}/\sigma_{CH}/[n_C] \rightarrow r_{C(3p_x)}$	291.5	327.6
$CH_2O(9) \rightarrow HCO^-(9) + H^+$ $^1B_1 \qquad ^1A''$	$\pi_{CO} \rightarrow r_{C(3s)}$	344.7	341.6
Triplet states $CH_2O(1) \rightarrow HCO^-(5) + H^+$ $^3A_2 \qquad ^1A''$	$n_{O(2p_x)}/[n_C] \rightarrow \pi_{CO}^*$	414.7	413.2
$CH_2O(2) \rightarrow HCO^-(6) + H^+$ $^3A_1 \qquad ^1A'$	$\pi_{CO} \rightarrow \pi_{CO}^*$	422.2	427.8
$CH_2O(3) \rightarrow HCO^-(2) + H^+$ $^3B_2 \qquad ^1A'$	$n_{O(2p_x)}/[n_C] \rightarrow r_{C(3s)}/\sigma_{CH}^*$	275.0	374.2
$CH_2O(4) \rightarrow HCO^-(1) + H^+$ $^3B_1 \qquad ^1A''$	$n_{O(2p_x)}/[n_C] \rightarrow \pi_{CO}^*/\sigma_{CO}^*$	231.9	264.5
$CH_2O(6) \rightarrow HCO^-(10) + H^+$ $^3A_1 \qquad ^1A'$	$n_{O(2p_x)}/\sigma_{CH}/[n_C] \rightarrow r_{C(3p_x)}/r_{O(3p_x)}$	387.1	388.5

than in the acid; however, many of those in the base are excitations out of the additional lone pair not common to both species. For example, the CH_2CH^- carbon lone pair is not present in ethylene. If one considers only those states common to both species, such as the ones connected by dot-
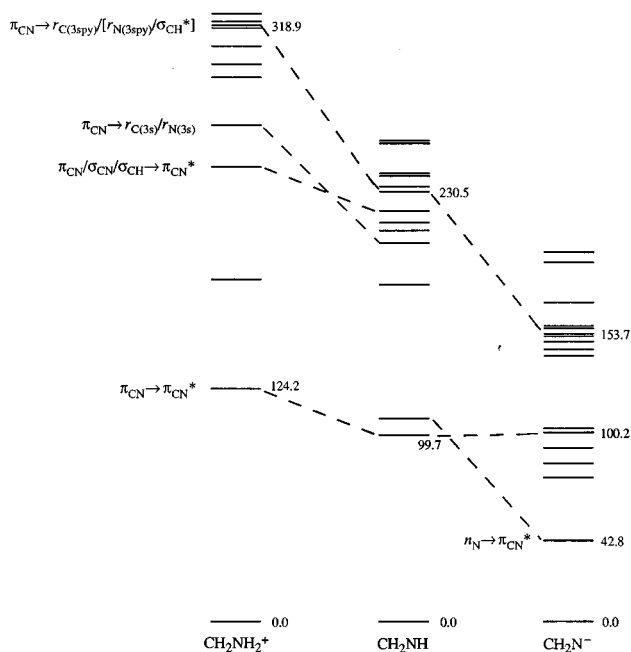

FIG. 5. Triplet state vertical transition energies (in kcal/mol) for the CH_2NH_n series. Selected states for which a vertical deprotonation energy can be found are connected with dotted lines.

ted lines in Fig. 5, the spacing of the excited states results in a general reduction of VEE as the system is progressively deprotonated. With one exception, the ordering of excited states of similar character is the same unless the states are close together in both species.

The one type of transition which does not follow the above trends is the $\pi \rightarrow \pi^*$ state. In some cases, this state undergoes little or no stabilization in the deprotonated species, as compared to the protonated one. An example is exhibited in Fig. 5, where the VEE of the $\pi \rightarrow \pi^*$ state in21 CH_2N^- is in fact slightly larger than in its parent CH_2NH. This behavior contrasts sharply with the lowering of most other states upon deprotonation. This is true of all the triplet and some singlet $\pi \rightarrow \pi^*$ states of the anions. The same phenomenon is noted in some singlet $\pi \rightarrow \pi^*$ states of neutral species as compared to their parent cation.

Investigation as to which MOs are involved in the $\pi \rightarrow \pi^*$ excitations which exhibit this phenomenon reveals that these excitations are indeed mostly of π character, but also contain contributions from MOs with some σ character. This contribution is also clearly seen in the occupancy changes of the σ-type NBOs, which are sometimes almost as great as those of the π and π^* orbitals. For example, in the case of the second triplet state listed in Table X ($\pi_{CN}/\sigma_{CN}/\sigma_{CH} \rightarrow \pi_{CN}^*$), Fig. 5 shows that in the deprotonated species, CH_2NH, the state of this character, while lower in excitation energy than that of $CH_2NH_2^+$, is higher in order for CH_2NH (state 7) than for $CH_2NH_2^+$ (state 3). In addition to shifting density in the out-of-plane π region from X_2 to C_1, density is depleted from the in-plane lone pair of X_2 and one or more hydrogens to regions further from the

molecule. Such shifts appear to destabilize the excited state more than pure $\pi\rightarrow\pi^*$ states in which this mixing does not occur. In the deprotonation reaction, this destabilization of the deprotonated species counteracts the general decrease in VEE accompanying the more negative net charge on the species, leading to a greater vertical deprotonation energy than the ground state DE, particularly for the CH_2CH_2, CH_2NH, and CH_2O triplet $\pi\rightarrow\pi^*$ states.

Next we compare the effect of geometry relaxation on the process by comparing the vertical with the adiabatic DEs. There are four general types of geometry relaxation that occur after excitation of $H_2C=XH_n$ species: changes in bond lengths (primarily r_{CX}), changes in bond angles (primarily θ_{CXH}), ''twisting'' of the XH_n group relative to CH_2, and pyramidal distortion of the CH_2 group. Table I shows that the adiabatic excitation energies of the ethylene $1\,^1B_{1u}(V)$ and $1\,^3B_{1u}(T)$ states have been lowered by 49.3 and 36.2 kcal/mol, respectively, relative to the corresponding VEE values by twisting nearly 90° [Fig. 2(a)]. The adiabatic transition energy of $2\,^3B_{2g}$ state [Fig. 2(c)], is 55.1 kcal/mol lower due to an asymmetric pyramidal distortion of the CH_2 groups. Nearly the same energy lowering, 46.4 kcal/mol, occurs for the planar $2\,^1B_{2g}$ state, but in this case by a severe elongation of the CC bond by 0.31 Å. Twisting by 38.4° lowers the energy of the $3\,^1A''$ state of CH_2NH (Table IV) by 25.8 kcal/mol, while pyramidal distortion stabilizes several states by more than 40 kcal/mol. Closure of the θ_{CNH} angle from 112° to 90° with a slightly shorter CN bond stabilizes the $4\,^1A'$ state by 23.6 kcal/mol, while opening it up to 144° lowers the $4\,^3A'$ state energy by 17.1 kcal/mol. Bond length changes of less than 0.1 Å and angle changes less than 10° for other planar states lower the energy by only ~5–15 kcal/mol. Correlation of the amount of energy lowering with geometry changes in all eight species in this study yields the following stabilization hierarchy:

$$\Delta r_{CX}\approx\Delta\theta_{CXH}$$

$$<\text{pyramidal distortion}<\text{twist}<\text{twist}+\text{pyramidization}.$$

Comparison of the major geometry changes of the protonated and deprotonated species upon relaxation explains the differences between the vertical and adiabatic excited state deprotonation energies. A greater geometric stabilization of the protonated species causes $E_i^A(BH^+)$ to be lower relative to $E_j^A(B)$, and hence the adiabatic deprotonation energy is greater than the VDE; the opposite is true if the deprotonated species is more stabilized. For the $n\rightarrow\pi^*$, $n\rightarrow r_{3p_z}$ (out-of-plane Rydberg), all but one of the $\pi\rightarrow\pi^*$, and several of the $\pi\rightarrow r_{3p_z}$ and $\pi\rightarrow r_{3p_y}$ states, the optimized geometry of the protonated species shows nearly equal or greater twist or pyramidal distortion than does the deprotonated species. In several cases the increase of the deprotonation energy due to geometry relaxation is greater than is the lowering due to the change in the electron distribution (vertical properties), so the adiabatic deprotonation energy is even greater than that of the ground state. For the $\sigma\rightarrow\pi^*$ singlet and triplet states of ethylene, on the other hand, the deprotonated species (CH_2CH^-) is more distorted, so the

ADE is less than the VDE and is much smaller than the ground state deprotonation energy. The geometries of the acid and base are both planar for $\pi\rightarrow r_{3p_x}$, $n\rightarrow r_{3p_x}$, and $n\rightarrow r_{3p_y}$ states, so the adiabatic deprotonation energy is within ±20 kcal/mol of the VDE; the ADE is lower than the ground state deprotonation energy mainly due to the electronic effect.

V. CONCLUSIONS

Natural bond orbital analysis of CIS ground and excited state densities has been used to examine changes in bonding patterns upon excitation. This allows excited states of similar character in the acid and base to be correlated. The nature of the bonding NBOs that are depopulated and those antibonding or Rydberg orbitals that are populated can also be used to predict qualitative bond length and bond angle changes, including likely bond dissociations. In the case of planar molecules, the degree to which the excitation involves π or π^* MOs also determines the amount of nonplanar twisting or pyramidalization the system undergoes. NBO analysis shows that higher energy transitions are also more delocalized. Moreover, as the C–X electronegativity difference becomes greater, the excitations become more delocalized, and show more involvement of the σ_{CX}, σ_{CH}, and σ_{XH} bonds and antibonds. This greater contribution of the σ system to excitations leads to more frequent dissociation upon geometry relaxation.

The vertical transition energies of the deprotonated species tend to be lower and closer together than those of the protonated species. Therefore, most of the vertical deprotonation energies are less than the ground state DE. The calculations show evidence of a consistent charge shift away from the more electronegative atom upon excitation, which, independent of geometry relaxation, causes the species to be more easily deprotonated in the excited state than in the ground state in most cases. This shift becomes greater as the electronegativity difference between C and X increases. The exception is some $\pi\rightarrow\pi^*$ transitions, in which the VDE is higher than the ground state value because the excitation energy of the deprotonated species (anion or neutral) is higher than expected due to contributions from MOs with some σ-character which shift density away from the in-plane lone pair and hydrogens to regions further from the molecule.

Changes in geometry upon relaxation generally have a greater effect on the adiabatic deprotonation energies than shifts in the electron density, with pyramidal distortion and out-of-plane twisting more important than in-plane bond length and bond angle changes. The ADE may be greater or less than the VDE depending on whether the protonated or deprotonated species is more stabilized by geometry relaxation. Rydberg excited states, whose geometries generally remain planar, tend to decrease the deprotonation energy by removing electron density from the compact region about the heavy atom to which it is bonded. Unlike the adiabatic excited states in the $HC\equiv CH/HC\equiv C^-$ and $HC\equiv N/C\equiv N^-$ systems, those of the $H_2C=XH_2$ species tend to be ordered

and spaced differently in the protonated and deprotonated species, and so excited state deprotonation energies can be up to ~100 kcal/mol greater or less than the ground state deprotonation energy. The reordering is primarily caused by nonplanar distortion, which does not occur in these triply bonded systems.

These results are important in the context of proton transfer. To photocatalyze a rapid proton transfer, increasing the rate, one wishes to decrease the deprotonation energy or proton affinity of the proton donor, and increase that of the acceptor. In many cases this could be achieved experimentally by simultaneously exciting the donor to a low-lying Rydberg state and the acceptor into the π^* orbital, providing the adiabatic geometry of the system allows a lower barrier. Since adiabatic geometry strongly influences the deprotonation energies, knowledge of the excited state deprotonation energies in a comprehensive set of useful prototype fragments of common biological molecules with analogous geometries can show how local geometry influences excited state proton transfer for the larger systems.

ACKNOWLEDGMENT

[1] E. F. Caldin and V. Gold, *Proton-Transfer Reactions* (Halsted, New York, 1975); R. Stewart, *The Proton: Applications to Organic Chemistry* (Academic, Orlando, 1985).

[2] J. Rucker, Y. Cha, T. Jonsson, K. L. Grant, and J. P. Klinman, Biochemistry **31**, 11489 (1992); A. J. Beveridge and G. C. Heywood, *ibid*. **32**, 3325 (1993); I. A. Rose and D. J. Kuo, *ibid*. **31**, 5887 (1992); D. N. Silverman and S. Lindskog, Acc. Chem. Res. **21**, 30 (1988).

[3] M. Eigen, Angew. Chem. Int. Ed. Eng. **3**, 1 (1964); L. Onsager, Science **166**, 1359 (1969).

[4] L. G. Arnaut and S. J. Formosinho, J. Photochem. Photobiol. A **75**, 1 (1993); S. J. Formosinho and L. G. Arnaut, *ibid*. **75**, 21 (1993); D. A. Parthenopolous, D. McMorrow, and M. Kasha, J. Phys. Chem. **95**, 2668 (1991); G. A. Brucker, T. C. Swinney, and D. F. Kelley, *ibid*. **95**, 3190 (1991); J. Syage and J. Steadman, J. Chem. Phys. **95**, 2497 (1991); P.-T. Chou, M. L. Martinez, and W. C. Cooper, J. Am. Chem. Soc. **114**, 4943 (1992); T. Arthen-Engeland, T. Bultmann, N. P. Ernsting, M. A. Rodriguez, and W. Thiel, Chem. Phys. **163**, 43 (1992).

[5] CIS: J. B. Foresman, M. Head-Gordon, J. A. Pople, and M. J. Frisch, J. Phys. Chem. **96**, 135 (1992).

[6] MCSCF: B. O. Roos, in *Methods in Computational Molecular Physics*, edited by G. H. F. Diercksen and S. Wilson (Reidel, Dordrecht, 1983), p. 161; J. Olsen, D. L. Yeager, and P. Jorgenson, in *Advances in Chemical Physics*, edited by I. Prigogine and S. A. Rice (Wiley Interscience, New York, 1983), Vol. LIV, p. 1; H.-J. Werner and R. Shepard, in *Advances in Chemical Physics*, edited by K. P. Lawley (Wiley Interscience, New York, 1987), Vol. LXIX.

[7] MP2: C. Møller and M. S. Plesset, Phys. Rev. **46**, 618 (1934); J. S. Binkley and J. A. Pople, Int. J. Quantum Chem. Symp. **99**, 4899 (1977).

[8] S. Nagaoka, A. Itoh, K. Mukai, E. Hoshimoto, and N. Hirota, Chem. Phys. Lett. **192**, 532 (1992); S. Roszak, U. Kaldor, D. A. Chapman, and J. J. Kaufmann, J. Phys. Chem. **96**, 2123 (1992); Z. Latajka and S. Scheiner, *ibid*. **96**, 9764 (1992).

[9] M. Kasha, Discuss. Faraday Soc. **9**, 14 (1950).

[10] K. B. Wiberg, C. M. Hadad, J. B. Foresman, and W. A. Chupka, J. Phys. Chem. **96**, 10756 (1992).

[11] L. Serrano-Andres, M. Merchán, I. Nebot-Gil, R. Lindh, and B. O. Roos, J. Chem. Phys. **98**, 3151 (1993).

[12] E. R. Davidson and L. E. McMurchie, in *Excited States*, edited by E. C. Lim (Academic, New York, 1982), Vol. 5.

[13] J. Cioslowski, Int. J. Quantum Chem. **39**, 681 (1991).

[14] C. M. Hadad, J. B. Foresman, and K. B. Wiberg, J. Phys. Chem. **97**, 4293 (1993).

[15] M. Head-Gordon, R. J. Rico, M. Oumi, and T. J. Lee, Chem. Phys. Lett. **219**, 21 (1994).

[16] Y. Dimitrova and S. D. Peyerimhoff, Chem. Phys. Lett. **227**, 384 (1994).

[17] A. J. Merer and R. S. Mulliken, Chem. Rev. **69**, 639 (1969), and references therein.

[18] M. B. Robin, *Higher Excited States in Polyatomic Molecules* (Academic, New York, 1985), Vol. III, pp. 253–260.

[19] J. Chandresekhar, J. G. Andrade, and P. v. R. Schleyer, J. Am. Chem. Soc. **103**, 5609 (1981), and references therein.

[20] S. Olivella, F. Urpi, and J. Vilarrasa, J. Comput. Chem. **5**, 230 (1984).

[21] M. J. S. Dewar and K. M. Dieter, J. Am. Chem. Soc. **108**, 8075 (1986).

[22] G. P. Ford and J. D. Scribner, J. Comput. Chem. **4**, 594 (1983).

[23] J. E. Del Bene, J. Comput. Chem. **6**, 296 (1985).

[24] J. L. Ozment and A. M. Schmiedekamp, Int. J. Quantum Chem. **43**, 783 (1992).

[25] P. Burk, K. Herodes, I. Koppel, and I. Koppel, Int. J. Quantum Chem. Symp. **27**, 633 (1993).

[26] P. Speers and K. E. Laidig, J. Chem. Soc. Perkin Trans. II **4**, 799 (1994).

[27] B. J. Smith and L. Radom, Chem. Phys. Lett. **231**, 345 (1994).

[28] B. J. Smith and L. Radom, J. Am. Chem. Soc. **115**, 4885 (1993).

[29] J. F. Gal, I. Leito, P. C. Maria, E. D. Raczyńska, R. W. Taft, and F. Anvia, J. Chim. Phys. **92**, 22 (1995).

[30] V. Marudarajan and S. Scheiner, J. Phys. Chem. **95**, 10280 (1991).

[31] V. Marudarajan and S. Scheiner, Chem. Phys. Lett. **186**, 356 (1991).

[32] (a) J. P. Foster and F. Weinhold, J. Am. Chem. Soc. **102**, 7211 (1980); (b) A. E. Reed and F. Weinhold, J. Chem. Phys. **78**, 4066 (1983); (c) A. E. Reed, R. B. Weinstock, and F. Weinhold, *ibid*. **83**, 735 (1985); (d) A. E. Reed and F. Weinhold, *ibid*. **83**, 1736 (1985). Reviews: (e) A. E. Reed, L. A. Curtiss, and F. Weinhold, Chem. Rev. **88**, 899 (1988); (f) F. Weinhold and J. E. Carpenter, in *The Structure of Small Molecules and Ions*, edited by R. Naaman and Z. Vager (Plenum, New York, 1988).

[33] NBO Program Version 4.0: E. D. Glendening, J. K. Badenhoop, A. E. Reed, J. E. Carpenter, and F. Weinhold, Theoretical Chemistry Institute, University of Wisconsin, Madison, WI, 1994. F. Weinhold, NBO 4.0 Program Manual (University of Wisconsin Theoretical Chemistry Institute, Madison, 1994). NBO Program Version 3.0: E. D. Glendening, A. E. Reed, J. E. Carpenter, and F. Weinhold, QCPE Bull. **10**, 58 (1990); A. E. Reed and F. Weinhold, *ibid*. **5**, 141 (1985).

[34] GAUSSIAN 92 Revision F.2: M. J. Frisch, G. W. Trucks, M. Head-Gordon, P. M. W. Gill, M. W. Wong, J. B. Foresman, B. G. Johnson, H. B. Schlegel, M. A. Robb, E. S. Repogle, R. Gomperts, J. L. Andres, K. Raghavachari, J. S. Binkley, C. Gonzalez, R. L. Martin, D. J. Fox, D. J. Defrees, J. Baker, J. J. P. Stewart, and J. A. Pople, Gaussian, Inc., Pittsburgh, PA, 1992.

[35] P. C. Hariharan and J. A. Pople, Theor. Chim. Acta **28**, 213 (1973); J. D. Dill and J. A. Pople, J. Chem. Phys. **62**, 2921 (1975); T. Clark, J. Chandrasekhar, G. W. Spitznagel, and P. v. R. Schleyer, J. Comput. Chem. **4**, 294 (1983).

[36] J. Chandrasekhar, J. G. Andrade, and P. v. R. Schleyer, J. Am. Chem. Soc. **103**, 5609 (1981); G. W. Spitznagel, T. Clark, J. Chandrasekhar, and P. v. R. Schleyer, J. Comput. Chem. **3**, 363 (1982); D. J. DeFrees and A. D. McLean, *ibid*. **7**, 321 (1986).

[37] Z. Latajka and S. Scheiner, Chem. Phys. Lett. **105**, 435 (1984).

[38] Z. Latajka, S. Scheiner, and G. Chalasinski, Chem. Phys. Lett. **196**, 384 (1992).

[39] J. M. L. Martin, J. P. François, and R. Gijbels, J. Comput. Chem. **10**, 346 (1989).

[40] L. E. McMurchie and E. R. Davidson, J. Chem. Phys. **7**, 2959 (1977).

[41] J. E. Del Bene, R. Ditchfield, and J. A. Pople, J. Chem. Phys. **55**, 2236 (1971); R. Ditchfield, J. E. Del Bene, and J. A. Pople, J. Am. Chem. Soc. **94**, 703 (1972).

[42] Pyridine and porphin: Ref. 5. Bicyclo[1.1.0]butane: V. A. Walters, C. M. Hadad, Y. Thiel, S. D. Colson, K. B. Wiberg, P. M. Johnson, and J. B. Foresman, J. Am. Chem. Soc. **113**, 4782 (1991). 1,3-Butadiene: K. A. Wiberg, C. M. Hadad, G. B. Ellison, and J. B. Foresman, J. Phys. Chem. **97**, 13586 (1993).

[43] I. Mayer, J. Mol. Struct. (Theochem) **255**, 1 (1992).

[44] For a discussion of some problems associated with the use of nonorthogonal orbitals, see F. Weinhold and J. E. Carpenter, J. Mol. Struct. (Theochem) **165**, 189 (1988). In particular, anomalous unphysical population values (<0.00 or >2.00) violating the Pauli principle are found to

increase sharply with the degree of orbital overlap [R. S. Mulliken and W. C. Ermler, *Diatomic Molecules: Results of Ab Initio Calculations* (Academic Press, New York, 1977), pp. 33–38]. Though natural population analysis [Ref. 32(c)] has been shown to give stable populations for ground state densities, orthogonalization of the distorted and highly overlapping excited state CIS AOs yields similar anomalies. Almost all CIS densities produced orbitals within an established occupancy limit of $-0.01 < \rho < 2.01$ e; states yielding occupancies outside this limit were not considered.

[45] Natural bond orbitals have been shown to be highly transferable among similar molecules in the ground state [J. E. Carpenter and F. Weinhold, J. Am. Chem. Soc. **110**, 368 (1988)], and for these transitions, NBOs describing relatively unaffected parts of the molecule are likewise transferable. For example, the overlap between the ground and excited state α_{CH} bonds for the first excited triplet ($\pi \to \pi^*$) state is 0.9997, while that for the π_{CC} bond in the sixth singlet ($\sigma_{CH} \to \pi^*$) state is 0.9998. Therefore, more compact NBO-based assignments are a direct indication of the similarity of the ground and excited state densities.

[46] R. J. Buenker and S. D. Peyerimhoff, Chem. Phys. Lett. **36**, 415 (1975).

[47] Reference 18, pp. 213–227.

[48] R. S. Mulliken, Acc. Chem. Res. **9**, 7 (1976); Chem. Phys. Lett. **46**, 197 (1977).

[49] P. D. Foo and K. K. Innes, J. Chem. Phys. **60**, 4582 (1974).

[50] All of the states which break the NH bonds populate one or both σ_{NH}^*

orbitals or depopulate one or both σ_{NH} bonds by more than about 0.3–0.4 e relative to the ground state.

[51] For example, this can be seen in the case of the singlet $n_{X_2} \to r_{C_1(3px_y)}$ excitation. In CH$_2$CH$^-$ ($4\,^1A'$), 0.886 e is depleted from the CH$_2$CH$^-$ lone pair, and the Rydbergs on C$_1$ and C$_2$ increase occupancy by 0.509 and 0.304 e, respectively, whereas in CH$_2$NH ($5\,^1A'$), 0.767 e depleted from the N lone pair is divided 0.641/0.087 between the corresponding C and N Rydbergs. Thus, the charge on C$_1$ becomes significantly more negative for this state in CH$_2$NH than CH$_2$CH$^-$ ($\Delta q_{C_1} = -0.532$ vs -0.389).

[52] For example, the increase in charge shift toward C$_1$ for the triplet $\pi \to \pi^*$ excitation ($\Delta q_{C_1} = +0.376$ for CH$_2$CH$^-$ $2\,^3A''$, -0.158 for CH$_2$NH $1\,^3A'$, and -0.738 in CH$_2$OH$^+$ $1\,^3A'$) is consistent with the relative percentage composition of the ground state π NBO from the C$_1$ vs X$_2$ $2p_z$ hybrids: 64:35 C$_1$/X$_2$ in CH$_2$CH$^-$, 42:58 in CH$_2$NH, and 31:69 in CH$_2$OH$^+$; the coefficients are reversed for the π^* orbital.

[53] S. G. Lias, J. E. Bartmess, J. L. Holmes, R. D. Levin, J. F. Liebman, and W. G. Mallard, J. Phys. Chem. Ref. Data **17**, Suppl. N1, 673 (1988).

[54] In Ref. 53, p. 663.

[55] P. Kebarle, Annu. Rev. Phys. Chem. **28**, 445 (1977).

[56] S. G. Lias, T. F. Liebman, and R. D. Levin, J. Chem. Phys. Ref. Data **13**, 695 (1984).

[57] F. A. Cotton, *Chemical Applications of Group Theory* (Wiley-Interscience, New York, 1971).